Huang *et al. Microstructures* **2025**, *5*, 2025021
DOI: 10.20517/microstructures.2024.86

Microstructures

Review

Open Access

Check for updates

Heterostructured multi-principal element alloys prepared by laser-based techniques

Jiani Huang[1], Wenqing Yang[1], Zhenguang Gao[1], Xu Hou[1], Xu-Sheng Yang[1,2]

[1]Department of Industrial and Systems Engineering, Research Institute for Advanced Manufacturing, The Hong Kong Polytechnic University, Hung Hom, Kowloon, Hong Kong, China.
[2]Hong Kong Polytechnic University Shenzhen Research Institute, Shenzhen 518060, Guangdong, China.

Correspondence to: Prof. Xu-Sheng Yang, Department of Industrial and Systems Engineering, Research Institute for Advanced Manufacturing, The Hong Kong Polytechnic University, Hung Hom, Kowloon, Hong Kong, China. E-mail: xsyang@polyu.edu.hk; Dr. Xu Hou, Department of Industrial and Systems Engineering, Research Institute for Advanced Manufacturing, The Hong Kong Polytechnic University, Hung Hom, Kowloon, Hong Kong, China. E-mail: jackie-xu.hou@polyu.edu.hk

How to cite this article: Huang, J.; Yang, W.; Gao, Z.; Hou, X.; Yang, X. S. Heterostructured multi-principal element alloys prepared by laser-based techniques. *Microstructures* **2025**, *5*, 2025021. https://dx.doi.org/10.20517/microstructures.2024.86

Received: 7 Sep 2024 **First Decision:** 4 Dec 2024 **Revised:** 14 Dec 2024 **Accepted:** 30 Dec 2024 **Published:** 24 Feb 2025

Academic Editor: Yandong Wang **Copy Editor:** Fangling Lan **Production Editor:** Fangling Lan

Abstract

Heterostructured materials, featured by two or more distinct zones with unique properties and intricate interactions at hetero-zone boundaries, showcase a remarkable strength-ductility synergistic effect for achieving superior mechanical properties surpassing their conventional homogeneous counterparts. Benefiting from the basic characteristics, such as complex composition, high configurational entropy and local distortion, multi-principal element alloys offer a fruitful playground for creating diverse heterostructures. Laser-based techniques such as laser surface treatment and laser additive manufacturing provide facile solutions with advantages such as high-energy density, rapid solidification rate, and precise control over processed zones and shapes, making them promising for the advancement of heterostructured multi-principal-element alloys. This review primarily highlights the nanoscale microstructural characteristics of various heterostructured multi-principal element alloys fabricated by laser-based techniques, along with their enhanced mechanical properties and other relevant service attributes. Moreover, it sheds light on the challenges and opportunities in harmonizing microstructural features to optimize the mechanical behavior of heterostructured multi-principal element alloys for industrial applications.

Keywords: Heterostructures, multi-principal-element alloys, laser surface treatment, additive manufacturing, mechanical properties, microstructures.

INTRODUCTION

Metallic materials with an exceptional combination of excellent mechanical performance and strong damage tolerance are highly desired for structural applications, such as aerospace engineering and energy-efficient vehicles[1]. Nanocrystalline metallic materials are well explored to possess much enhanced strength compared to their conventional coarse-grained counterparts, but they suffer from limited ductility. The trade-off between strength and ductility in materials is fundamentally governed by their microstructural characteristics, which influence plastic deformation and stress transfer mechanisms[2]. Stress transfer refers to how stress is distributed and transferred between different phases or components with distinct properties within a material system. Heterostructured materials, formed by two or more distinct zones with dramatically different properties, exhibit unique stress transfer behavior such as hetero-deformation induced (HDI) strengthening and strain hardening[3]. Specifically, the generation and interaction of back stress and forward stress would lead to additional strengthening and strain hardening, which can boost yield strength while maintaining and even improving ductility for alleviating the strength-ductility trade-off and approaching superior mechanical performance[3]. Releasing from the constraint of single regulation of grain boundaries, heterostructured materials involve abundant architectures including gradient structures[4-7], lamellar structures[8,9], dual/multi-phase structures[10,11], core-shell structures[12-15], *etc*.

The superior mechanical properties observed in heterogeneous microstructures are not surprising, as this phenomenon is widespread in nature[16]. For instance, biological organisms use gradient structures with multi-scale hierarchical features to enhance damage resistance and adaptability[17,18]. Man-made heterostructured materials, such as the Beilian steel swords from the Chinese Han Dynasty, can be traced back to the 2nd century AD[3,19]. Since the early 2000s, increasing attention has been focused on the fundamental concepts and properties of heterostructured materials, including their behaviors at the nanoscale[18,20-22]. With the advancement of manufacturing techniques such as deposition and 3D printing, researchers have been able to create increasingly complex heterostructures. In recent years, attention has shifted toward enhancing material properties by adjusting the composition and interface characteristics of heterostructures, and exploring their potential applications in various fields[23].

Microstructural heterogeneity is the key to obtaining superior mechanical performance and needs to be elaborately designed in heterostructured metallic materials. The interaction and coupling between the heterostructured zones occur near the hetero-zone boundaries, accommodating strain gradient and leading to a synergistic effect[24,25]. HDI strengthening and HDI strain hardening are activated in heterostructured materials to increase the yield strength and improve the ductility, where the strength-ductility trade-off is extensively alleviated or even avoided[25-27]. For instance, gradient nanoscale dislocation cells were introduced into a stable single-phase face-centered cubic structure through directional forging, resulting in a high-strength and ductile alloy that exhibits gradual and predictable changes in mechanical properties under strain[5]. This is attributed to dislocation-controlled plastic deformation, which generates numerous tiny stacking faults and twins. The coordination of different phases is another common way to enhance performance. Laser direct deposition was employed to create directional eutectic microstructures with ultra-fine layers[28]. Compared to the as-cast alloy, this method improved strength by about 60% (up to 1.2 GPa) in the loading direction, while maintaining elongation. The enhanced properties stem from the coordinated deformation between the body- and the face-centered cubic phases. Furthermore, many reported works have created hierarchical heterostructures by combining multiple processing techniques, advancing the enhancement. For example, through combined techniques of surface mechanical attrition treatment and magnetron sputtering, a gradient nanograin structure was created on the surface of magnesium alloy, followed by the deposition of a nano-dual-phase metallic glass film. The heterostructured material displays a unique blend of high strength and excellent ductility[29]. It was found that the material's toughness results

from multiple shear banding, crack inhibition in the nanocrystalline layers, and surface recrystallization after severe plastic deformation treatment.

Multi-principal element alloys [MPEAs, also called compositionally complex alloys, containing medium and high entropy alloys (M/HEA)] show a strong potential for achieving outstanding mechanical properties surpassing those of traditional structural alloys with only one or two main components[30-34]. Leveraging their basic characteristics of intricate composition[11], and local distortion, MPEAs offer a fruitful playground for creating intricate heterostructured architectures, which are typically uncommon in traditional structural alloys[11]. For instance, eutectic MPEAs can form hierarchical microstructures with dual-phase lamellar colonies, which greatly enhance mechanical performance[35]. In contrast to conventional alloys, MPEAs can exhibit a wider variety of arrangements of microstructural features, enhancing their mechanical properties. Traditional methods can provide uniform or easy heterostructured microstructures and are often more cost-effective for bulk production. However, heterostructured materials fabricated by traditional methods, such as mechanical plastic deformation[3,36-40], magnetron sputtering[41-43], and electrodeposition[44-46], often possess arbitrary variety and size of microstructures that are hard to precisely control down to the nanoscale. For example, the thickness of lamellae produced by conventional solidification processes typically ranges from micrometers to sub-micrometers[28,47,48], which constrains the achievable strengths of these equiatomic MPEAs. Metals with uniform microstructures of nanolayer and nano lamellar demonstrate high strength but often sacrifice ductility[27,49]. While traditional fabrication methods can yield highly textured nanostructures, they frequently lead to strong plastic anisotropy, limiting practical applications. These materials, often formed through techniques such as thin-film deposition or severe plastic deformation, struggle to achieve the desired overall balance of strength and ductility of complex shapes products due to their typical microstructural characteristics and processing limits[29].

Laser-based techniques including laser surface treatment (LST) and laser additive manufacturing (LAM) offer several advantages for producing heterostructured materials. The unique physical metallurgical properties of laser-based technologies, such as the high working temperature, extreme temperature gradients, and rapid solidification rates, facilitate the homogeneous precipitation of *in situ* nanophases[50-53]. This phenomenon is generally unattainable in conventional powder metallurgy processes, particularly for thermodynamic systems with limited capabilities. The precise control afforded by laser processing allows for the creation of tailored microstructures that enhance the mechanical properties of the resulting alloys[41,54-56]. For instance, laser processing has led to the development of innovative heterostructures, such as inverse gradient materials, dislocation networks and so on, exhibiting unique mechanical behaviors[57,58]. However, these methods can also introduce complexities such as thermal stresses and potential defects due to rapid cooling rates.

This review will first introduce various laser techniques and the diverse and highly adjustable heterostructures they produce. Then, we will summarize the nanoscale microstructural features of diverse heterostructured MPEAs engineered through laser-based techniques, along with their enhanced strength-ductility properties and other pertinent service attributes, aiming to deepen our understanding of how these structures influence mechanical and functional performance. Lastly, we will present an outlook on the current research landscape, offering perspectives on the precise design of heterostructures in MPEAs to achieve superior mechanical and service performance. By examining the design flow from laser-based techniques to material performance, this work explores the intricate balance of microstructural characteristics that govern the mechanical behavior of heterostructured MPEAs, with an overarching goal of leveraging these properties to inspire future structural materials. Notably, laser-manufactured heterogeneous MPEA components hold great promise across multiple industries, including surface

treatment in automotive, additive manufactured parts in aerospace, and biomaterials with tailored properties in biomedical fields, where their unique properties can be most effectively utilized[59].

LASER-BASED TECHNIQUES FOR CREATING HETEROGENEOUS STRUCTURES

The application of advanced and effective techniques is highly desired for creating heterostructured materials with precisely manipulated microstructural characteristics, targeting memorably enhanced mechanical properties. Among these methods, laser-based techniques are particularly notable for their precision and versatility. These techniques range from surface treatment processes to advanced manufacturing methods that allow precise control over materials at micro and nanoscales[60,61]. The following sections will focus on two key areas: laser-based surface treatment and additive manufacturing (AM). The former plays a critical role in enhancing surface properties by modifying the microstructure at the surface level, while the latter enables the creation of complex geometries and tailored material compositions with innovation in design and functionality.

Laser surface treatment

LST is widely used in materials science to prepare heterostructured surfaces on top of substrate materials. This technique offers high repeatability and controllability, enabling precise tailoring of processed parts to meet specific requirements. As shown in Figure 1, typical LST techniques are illustrated in three processing configurations according to the difference of raw materials and processing ways. By using laser energy as a heating source or shock wave, LST can control the area and depth of treatment with high accuracy, ensuring consistent quality and performance across various applications[62-64]. The technique is also beneficial in applications where traditional treatment methods may fall short, as it minimizes thermal distortion and allows for localized treatment without affecting the bulk material properties.

Laser surface remelting (LSR) uses a high-energy laser beam to quickly melt and solidify the surface of a material[65]. By adjusting the laser's scanning speed and power, it is possible to control the depth and extent of melting. Not only can LSR create surface layer structures, but also it can create surface gradient structures. A smooth transition in microstructure from the surface layer to the matrix can be achieved by LSR, resulting in excellent overall properties[66].

Laser glazing is similar to LSR but focuses on creating a thin, uniform layer on the surface, typically between 0.5 and 100 μm thick. This process involves very rapid cooling, often faster than 100,000 degrees per second, which helps form a glass-like or ultrafine grain structure[50]. Laser glazing can be engineered to produce thermal barrier coatings that are impermeable and resistant to surface corrosion and wear yet maintain porosity in the bulk. In contrast to the superficial layer created by laser glazing, LSR usually produces a deeper molten layer with a typical thickness between 100 and 500 μm, enhancing the ability to form more complex microstructure at localized areas. For instance, this deeper treatment is especially useful for developing gradient materials, where a change in microstructure and properties as desired will be precisely controlled along the building direction of processed materials.

Laser cladding (LC) is another cutting-edge technology used to modify the surface properties of materials. This technique involves depositing cladding material onto a substrate and using a high-energy laser beam to melt this additional material into a thin layer on top of substrate materials[67]. This process forms a metallurgically bonded layer. Metallic powders, typically delivered through coaxial or lateral nozzles, are commonly used in this method. The interaction between the metal powder and the laser beam generates a melt pool, which solidifies into a durable metal track as the substrate moves[68].

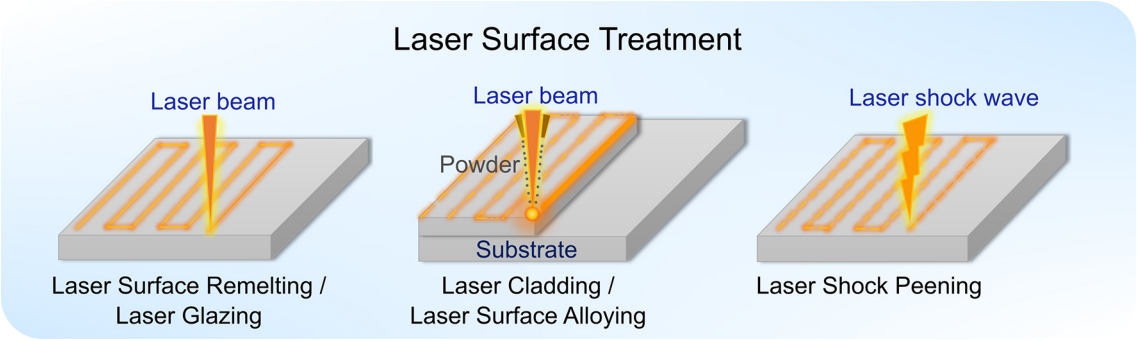

Figure 1. Processing configurations of typical LST techniques including laser surface remelting, laser glazing, laser cladding, laser surface alloying and laser shock peening.

Laser surface alloying, while resembling LC, primarily modifies the chemical composition of the substrate's surface and its immediate vicinity, rather than adding a distinct layer on top. This process is more complex and requires precise control over the laser parameters and the addition of alloying materials to achieve uniformity and optimal performance of the alloyed layer.

The alloying process includes melting, mixing, and rapid solidification[50]. The coatings that contain the alloying elements might be pre-applied using techniques such as electroplating or vapor deposition. During laser treatment, these pre-applied coatings are melted together with the substrate surface, allowing the alloying elements to integrate directly into the melt pool. In contrast, co-deposition refers to the simultaneous feeding of alloy powders or mixtures directly into the melt pool during laser processing. This method ensures that the alloying materials are introduced and mixed in real-time with the molten substrate, potentially offering more immediate and dynamic control over the composition and properties of the resulting alloyed layer. To achieve a uniform microstructure, both pre-deposition and co-deposition methods require overlapping the melting tracks by 20%-30%. This overlap ensures consistent properties throughout the laser-alloyed zone, which differs significantly from the substrate composition[50].

Laser shock peening (LSP), on the other hand, operates distinctly from other LST techniques by focusing on the mechanical rather than thermal effects. Unlike methods that rely on surface temperatures reaching T_m (the melting point), LSP is effective in avoiding the negative impacts of overmuch heating. During LSP, a plasma shock wave is generated through a high-power laser pulse[69]. When the material is irradiated by a high-power laser pulse, moderate-temperature and high-pressure plasma is instantly generated. The rapid expansion of this plasma creates a potent shock wave that propagates into the material, inducing high residual compressive stress and plastic deformation on the surface. Consequently, a gradient hardening layer is formed. Without the thermal damage and phase changes associated with higher temperature[69], this process creates near-surface compressive residual stresses and work-hardening states, which significantly improve resistance to crack initiation and propagation.

LSP is particularly well-suited for the preparation of heterostructured materials with a gradient distribution of hardness and strength, which is highly effective in enhancing the fatigue life of metallic materials[67]. The high-strain-rate deformation caused by the laser shock pressure (typically in the range of 10^5 to 10^7 s^{-1}) results in greater magnitude and depth of compressive residual stresses and higher strain-hardening ratios compared to other plastic deformation processes such as shot peening and deep rolling[70]. This makes LSP more effective and widely applied in industry.

Laser additive manufacturing

AM is a transformative approach to creating heterostructured materials by building parts layer by layer according to digital models. This technique allows for intricate designs and precise control over material composition and microstructure, making it ideal for fabricating complex, high-performance MPEA components[71-73].

Advancements in control systems have significantly enhanced the economic efficiency of producing parts via layer-by-layer AM techniques. LAM exemplifies this progress. As depicted in Figure 2, it is a technique that fabricates three-dimensional objects by sequentially adding material[74]. Selective laser melting (SLM) stands out as a prominent method within LAM, further showcasing the capabilities of this technology in precise and efficient manufacturing. First, the 3D model is decomposed into a series of two-dimensional layers that mimic the final product shape. Then, a laser beam scans these two-dimensional cross-sections, melting metal powder and forming particle bonds, layer by layer, to construct the final three-dimensional part[53,75]. The speed of SLM is generally slower than some other AM techniques due to the need for precise layer-by-layer scanning and residual stresses and warping may be introduced during the process, requiring post-processing sometimes.

Direct metal laser sintering (DMLS) is another key AM technique that utilizes a high-wattage laser to fuse powdered metals into solid structures. Unlike SLM, DMLS sinters the metal powder without completely melting it, which helps build objects layer by layer with fine detail and excellent surface finish[76]. This method is particularly useful for creating porous metal components and complex geometries. Additionally, DMLS can be adapted to sinter other materials such as ceramics and polymers, a process known as selective laser sintering (SLS). A major advantage of DMLS and SLS is their ability to produce parts with minimal residual stresses and internal defects due to partial melting, which are common drawbacks in traditionally manufactured components[67]. Nevertheless, when compared with SLM, the application scope of DMLS is relatively restricted. The reason is that the material density and mechanical properties obtained through DMLS are generally somewhat inferior.

Other common LAM methods include laser direct deposition (LDD). It is a type of Directed Energy Deposition, which covers a range of AM technologies that use energy sources such as lasers, electron beams, or plasma arcs. LDD involves directly feeding metal powder or wire material into the laser focal area, melting it, and depositing it onto the substrate to form layered structures[77,78]. It often uses higher laser speeds to maintain a continuous flow of material and rapid deposition, which can enhance build speed but may compromise precision and surface quality. This method is suitable for repairing and manufacturing complex parts[79]. By precisely controlling laser power, scanning speed, and powder supply parameters, different material compositions and performance variations can be achieved within the same component. For example, in SLM and LDD processes, gradient structures can be created by altering the type and proportion of powder material, resulting in diverse mechanical properties and corrosion resistance in different regions[74,80]. This is particularly important for manufacturing complex parts with high performance and multifunctionality.

When comparing these techniques, SLM typically involves slower laser speeds to ensure precise melting and solidification, leading to high accuracy but longer build times. This method often introduces residual stresses and warping, requiring post-processing. In contrast, DMLS/SLS uses moderate laser speeds, balancing between precision and build time, as sintering requires controlled heating but not complete melting. This results in fine details and excellent surface finishes with minimal residual stresses. LDD utilizes higher laser speeds to maintain a continuous flow of material and rapid deposition, enhancing build speed but potentially compromising precision and surface quality.

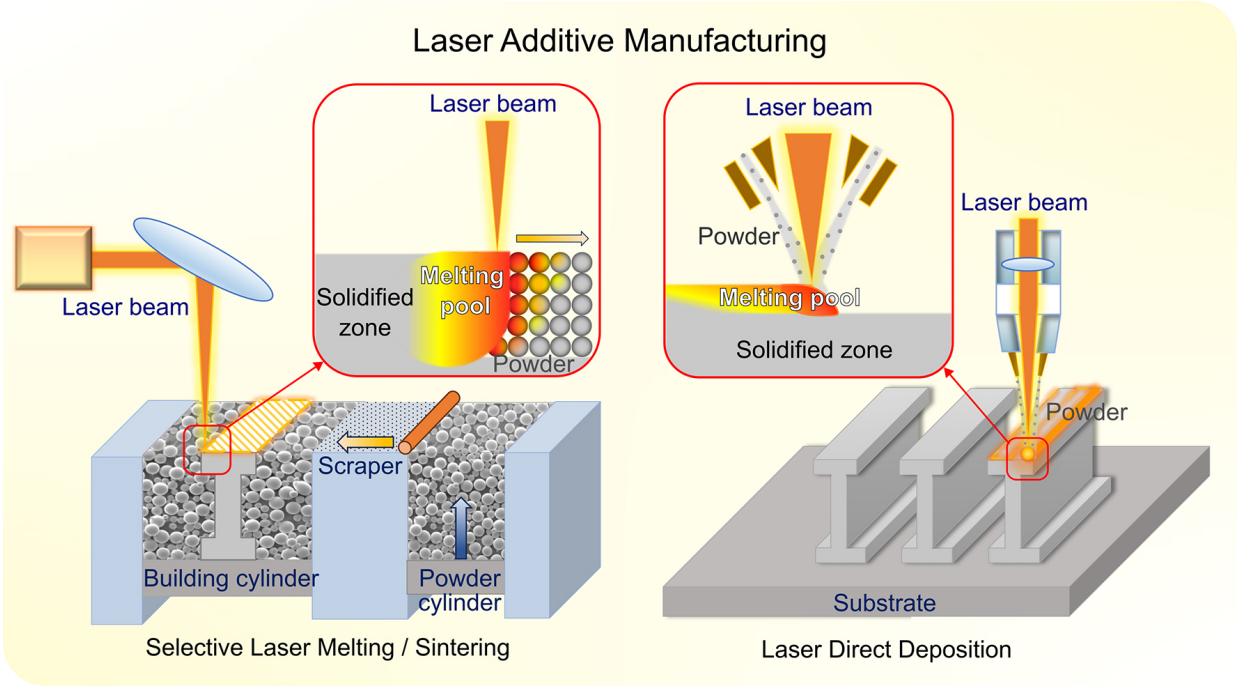

Figure 2. Effective LAM techniques for creating heterostructured materials including selective laser melting/sintering and laser direct deposition.

The AM technique is characterized by unique forming modes, such as melt pool connection, layer-by-layer deposition, high cooling rates, and nonequilibrium solidification. These processes often result in heterogeneous structures with distinctive features, including melt pools, columnar grains, lamellar structures, core-shell structures, phase heterogeneity, and nano-precipitation[24,52,81,82]. These microstructural characteristics contribute significantly to the enhanced mechanical properties and performance of the final components. While each laser-based AM technique offers distinct advantages, they also confront some specific challenges. These include issues related to residual stresses, porosity, and the need for post-processing to achieve desired surface finishes and dimensional accuracies. The choice of technique depends on the desired balance between precision, speed, material properties, and cost, making it essential to tailor the method to specific application requirements.

MICROSTRUCTURE CHARACTERISTICS IN HETEROSTRUCTURED MPEAS

The precise control of microstructure in heterostructured MPEAs is pivotal for realizing their exceptional mechanical properties. Advanced laser-based techniques have significantly developed beyond traditional methods, enabling fantastic achievements of novel microstructures more than ultra-fine grain sizes. These techniques introduce beneficial microstructures, which significantly enhance the mechanical performance of these alloys[83,84]. Conventional LST techniques, such as LC and laser surface alloying, can introduce entirely new coatings on the substrate surface, forming heterostructures that can effectively enhance the material's corrosion resistance and wear performance[85]. However, the formation of an ultra-thin layer on the top surface may contribute less to the overall mechanical performance. Herein, we focus on reviewing several heterostructures that largely improve mechanical properties, such as gradient structures, dual-phase or multi-phase structures, core-shell structures, skeleton architectures, lamellar structures, nano precipitates, and hierarchical heterogeneous structures, as shown in Figure 3. These heterostructures can simultaneously improve both the surface performance and overall mechanical properties of the material.

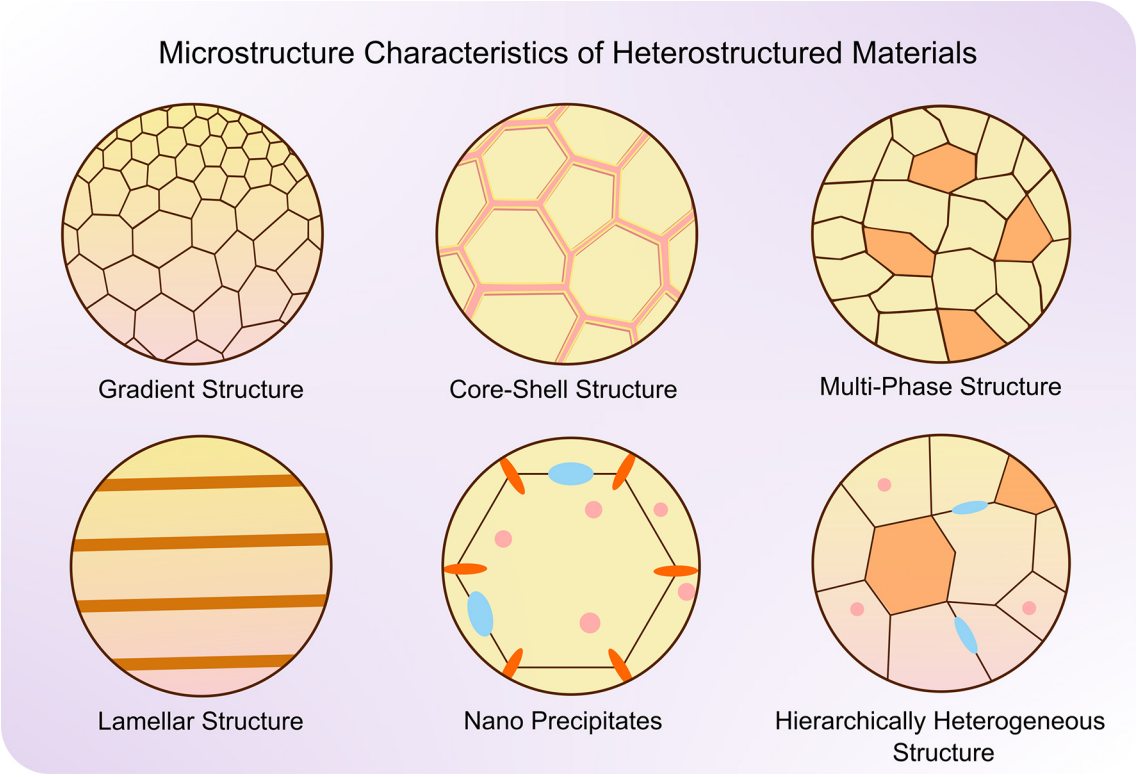

Figure 3. Typical heterostructures fabricated by laser-based techniques, such as gradient structure, core-shell structure, dual-phase or multi-phase structure, lamellar structure, nano precipitates, and hierarchical heterogeneous structure.

Gradient structure

A grain size gradient is one of the typical characteristic features of gradient materials. As a traditional mechanical method, severe surface plastic deformation is commonly employed to refine surface grains, resulting in an increasing grain size gradient from the surface to the center. LSP operates on a similar principle. The study by Fu *et al.* confirmed the effectiveness of LSP in introducing gradient structures to enhance the mechanical properties of MPEAs[86]. As illustrated in Figure 4A and B, the LSP-treated $CrFeCoNiMn_{0.75}Cu_{0.25}$ MPEA develops a hardened surface layer of several hundred micrometers thick. Notably, the sample that goes through four cycles of LSP treatment exhibits significant surface grain refinement and marked improvements in mechanical properties.

Another widely used laser treatment method is LSR. Unlike LSP, which typically produces a thin surface layer composed of fine crystals, LSR generates a thick molten layer due to the greater penetration depth of the laser. The resulting gradient structure is highly dependent on the specific laser parameters employed. Yuan *et al.* demonstrated that LSR can produce a hardened and corrosion-resistant surface layer in a fully recrystallized $(CrCoNi)_{92}Si_4B_4$ MPEA[87], as illustrated in Figure 4C. The microstructure observed includes characteristically oriented columnar grains, perpendicular to the molten pool boundary, with an average grain size of approximately 25 μm - significantly larger than that of the original base material [Figure 4D].

By combining laser processing with deformation, researchers have linked the resulting gradient structure to recovery and recrystallization, resulting in distinct structures. Zhang *et al.* achieved inverse gradient grain CoCrFeMnNi MPEAs, demonstrating exceptional strength-ductility combinations through a cold rolling-laser surface heat treatment method, which shows a grain size progression from the tough core to the soft

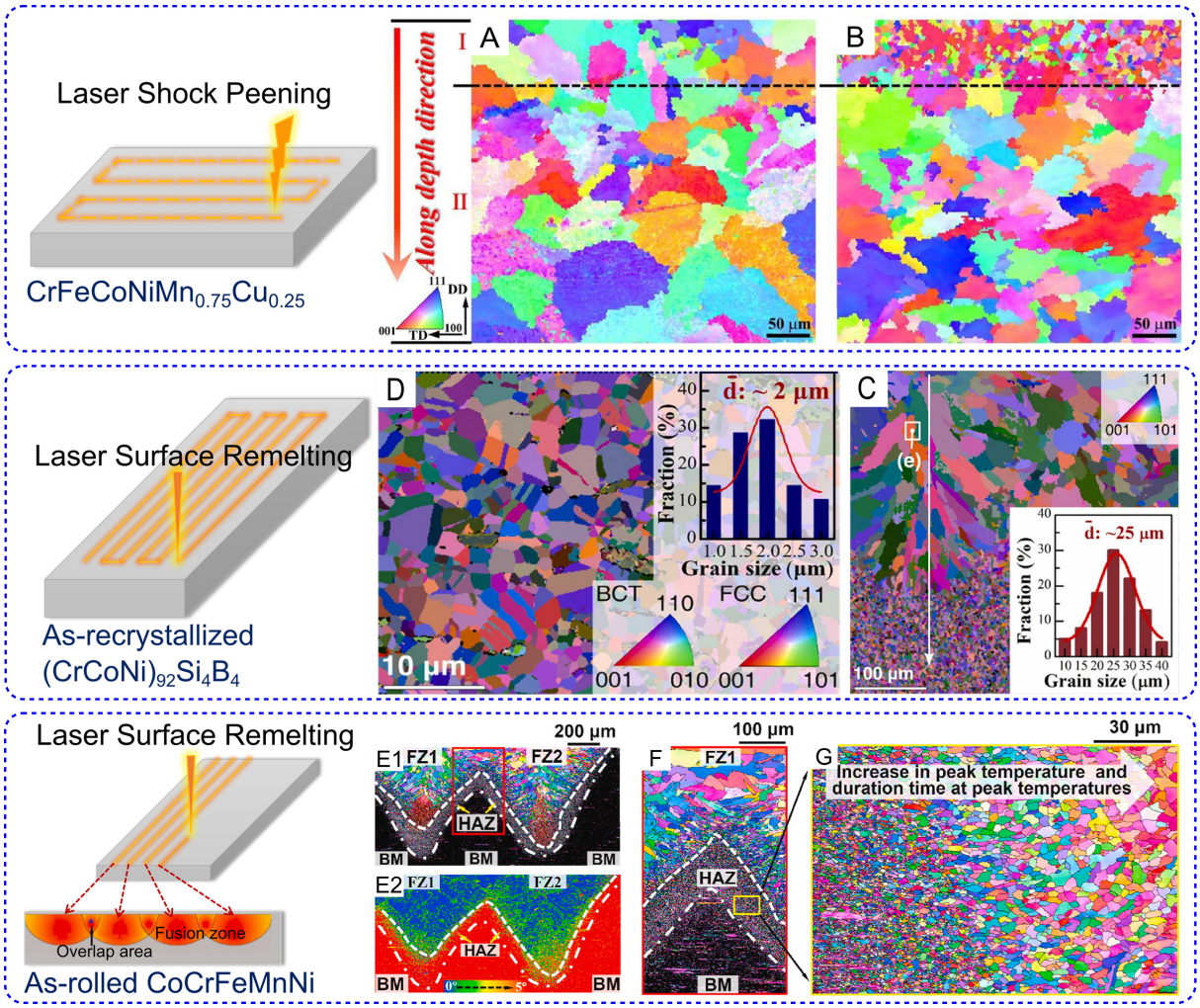

Figure 4. Gradient structures created by LST techniques: (A and B) Cross-sectional EBSD images of $CrFeCoNiMn_{0.75}Cu_{0.25}$ MPEA processed by 1 and 4 cycles of LSP, respectively[86]. (C and D) Grain size distribution of as-fully recrystallized $(CrCoNi)_{92}Si_4B_4$ MPEA after and before LSR[87]. (E1 and E2) grain distribution of inverse gradient LSR-CoCrFeMnNi, more details are given in (F) and (G) for clear view of local microstructures containing heat-affected zone (HAZ) and fusion zone (FZ)[89].

surface[88]. Subsequently, Shen *et al.* employed LSR on cold-rolled CoCrFeMnNi MPEAs using single and double-sided laser passes[89]. As shown in Figure 4E-G, the single-sided laser-treated MPEA exhibits a heterogeneous gradient structure as follows: (i) coarse columnar grains in the fusion zone; (ii) coarser grains in the heat-affected zone adjacent to the fusion zone, compared to the base material; (iii) a mix of smaller revertant and fine recrystallized grains in the HAZ near the base material; and (iv) distinct highly deformed pancake-like grains.

Building on the concept of inverse gradient, a thicker inverse gradient layer can be achieved through LDD, also known as laser metal deposition. This process involves laser treatment and powder melting deposition. LDD is particularly effective in manufacturing gradient structures because it allows for the controlled deposition of the same or different materials within a single component.

In the study by Gu *et al.*, LDD was applied to heavily cold-rolled CoCrFeMnNi sheets, resulting in a material with a combination of different grain structures across its depth[90]. This includes four distinct

regions: a coarse-grained outer layer, a transitional layer with columnar grains, an inner fine-grained layer, and a partially recrystallized core featuring nanosized grains, as depicted in Figure 5A-C. This strategic manipulation of thermal gradients during LDD leads to a specific reverse gradient structure.

Thanks to the precise control offered by the laser control system, LDD can achieve a chemical composition gradient by varying the composition of the deposited material. Dobbelstein *et al.* produced compositional gradient refractory MPEAs for screening purposes by *in-situ* alloying of elemental powder mixtures[91]. By gradually replacing Zr powder with Nb powder, they obtained a compositional gradient from $Ti_{25}Zr_{50}Nb_{0}Ta_{25}$ to $Ti_{25}Zr_{0}Nb_{50}Ta_{25}$. As shown in Figure 5D, the mean grain size of the body-centered cubic matrix increases from approximately 2 μm for $Ti_{25}Zr_{50}Nb_{0}Ta_{25}$ near the Mo-substrate to about 60 μm for $Ti_{25}Zr_{0}Nb_{50}Ta_{25}$ at the tip of the wall structure, which is more influenced by the chemical segregation of Ta in Zr-rich regions than by the cooling rate.

Dual-phase or multi-phase structure

Different from the gradient structures with gradual changes in the composition or/and phases along one specific direction, dual-phase or multi-phase structure is another most common type of heretostructure. This structure not only allows for a more significant performance comparison between different phases but also enhances the toughness, strength, and corrosion resistance of the material through their interactions.

Building on the bidirectional diffusion behavior of Fe, Co, Cr, Ni, and W elements, along with the principles of lattice distortion, Guan *et al.* successfully prepared FeCoCrNi-W coatings featuring an *in situ* Laves phase and face-centered cubic dual-phase structure through LC[92]. The composition of the Laves phase decreases from 39.15% at the surface to 12.67% at the substrate, creating a heterogeneous structure that transitions from dual-phase to eutectic and hypoeutectic [Figure 6A-D]. The Laves phase contributes high hardness and deformation resistance, while the face-centered cubic phase offers excellent plastic deformation capability. This orderly arrangement of hard and soft phases enhances the overall performance of the coating.

For original single-phase MPEAs, laser processing can still facilitate phase transformation, introducing a multi-phase structure into the system and enhancing the synergy of mechanical properties. For instance, Luo *et al.* prepared gradient nanostructured (GNS) layers on TiZrHfTaNb MPEAs through LSR[93]. This process allows the original coarse-grained single-phase body-centered cubic TiZrHfTaNb refractory MPEA to gradually decompose into a TiNb-rich body-centered cubic phase, a TaNb-rich body-centered cubic phase, a ZrHf-rich hexagonal close-packed phase, and a TiZrHf-rich face-centered cubic phase. These phases exhibit a gradient distribution in grain size along the depth direction during the grain refinement process, as depicted in Figure 6E-L. The introduction of decomposed multi-phase and gradient nanostructures greatly improves the wear resistance of the alloy. The synergistic effect of these heterogeneous microstructures, spanning from nanometer to sub-millimeter scales, contributes to the alloy's superior properties.

Core-shell structure and skeleton architecture

When exploring the advantages of biphasic or polyphase structures, it is notable that core-shell structure materials have gradually become popular with the further development of material design. The core-shell structure owns more dense textures and provides a more flexible way to adjust performance by combining the excellent properties of different components at micro levels.

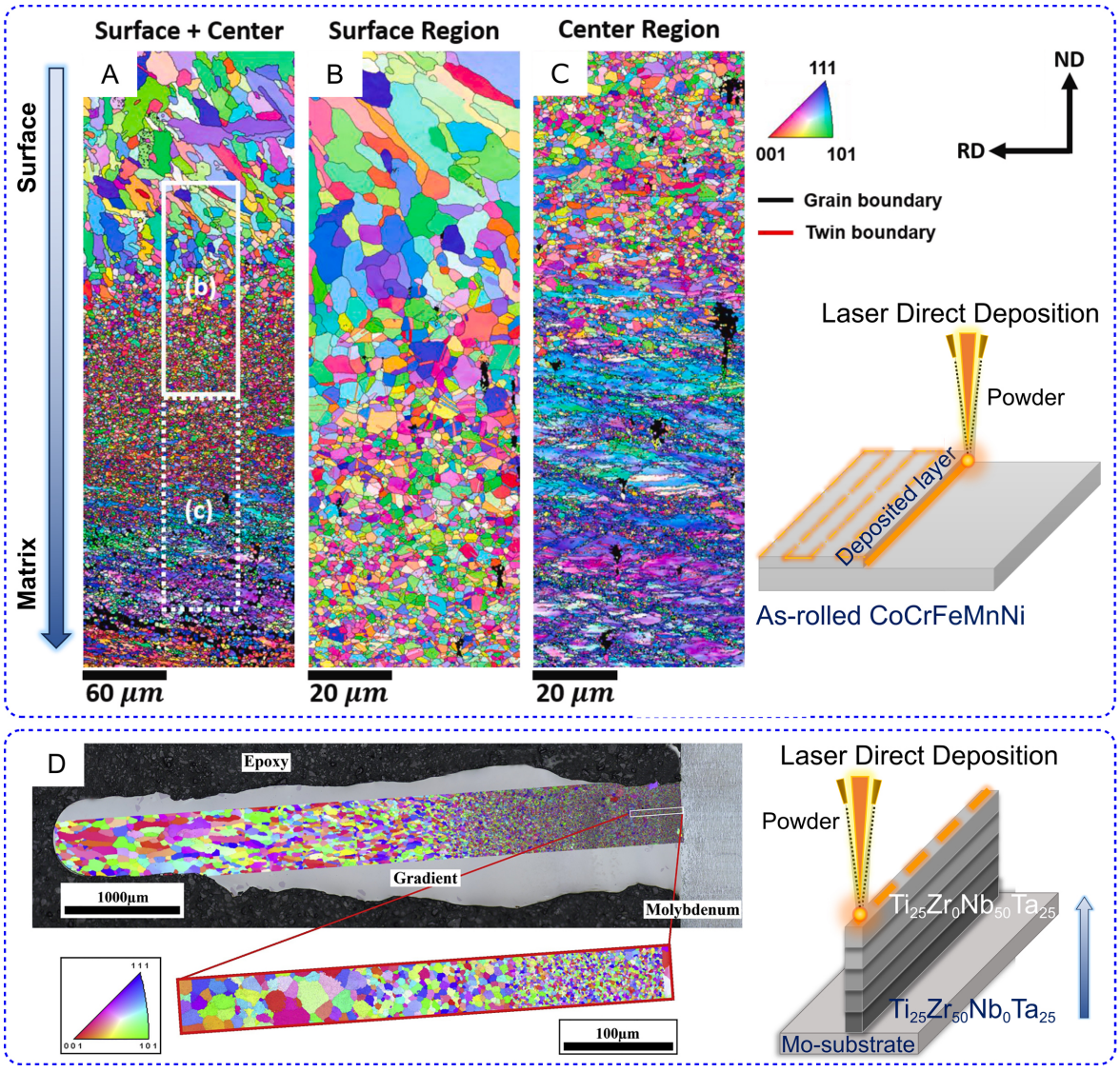

Figure 5. Gradient structures created by LAM techniques: Inverse pole figure (IPF) maps of inverse-gradient structured LDD-CoCrFeMnNi MPEA at (A) region including both the center and surface regions; (B) magnified region near the surface; and (C) magnified region near the center[90]. (D) Backscattered Electron (BSE) image with a grain orientation map obtained by EBSD of chemical composition gradient TiZrNbTa[91].

Zhang *et al.* fabricated an $AlCoCrFeNi_{2.1}$ eutectic MPEA featuring a unique composite core-shell structure through SLM[94]. This alloy exhibits a distinctive fish-scale microstructure, comprising ultrafine honeycomb and columnar sub-grains as shown in Figure 7A-H. It presents a dual-phase structure with face-centered cubic and B2 phases, where the B2 phase forms a unique shell configuration around the face-centered cubic phase cell. This specialized microstructure endows the alloy with high strength and good ductility, achieving impressive mechanical properties, including a tensile strength of 1,159.4 MPa and a plastic elongation of 29.0%.

Similarly, Kumar *et al.* employed SLM to fabricate $Al_{0.5}CrCoFeNi$ MPEAs, which display a face-centered cubic +B2 nano-bridged honeycomb structure[95] [Figure 7I-M]. The cell boundaries are formed by the B2 phase, interconnected by nano-bridges with a high dislocation density. The B2 phase contributes strength

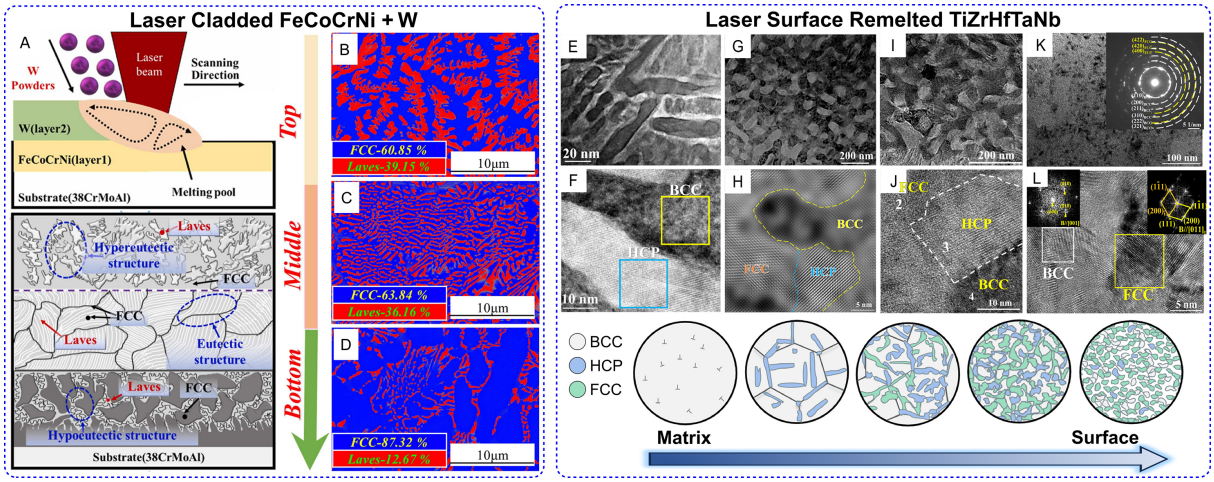

Figure 6. Dual-phase or multi-phase structures created by LST and LAM techniques: (A) The solidification process of LC-(FeCoCrNi + W) gradient composite coating and the microstructures formed in the corresponding coating layer; (B-D) Cross-sections showing the spatial distribution of face-centered cubic and laves phases of different depth of LC-(FeCoCrNi + W)[92]. (E-L) TEM characterization of the region at a depth of 40-60 μm (E and F); 30-40 μm (G and H); 20-30 μm (I and J) and less than 10 μm (K and L) below LSR treated TiZrHfTaNb surface[93].

through solid-solution strengthening and high dislocation density, while the nano-bridges of dislocations connecting the face-centered cubic cells provide pathways for dislocation movement away from the crack tip.

High-density dislocations are commonly observed in metals produced through AM, primarily believed to arise from the significant thermal stresses generated during the solidification process. Based on that, the dislocation-precipitate skeleton structure enhances the mechanical properties of the material by stabilizing the dislocations and controlling the distribution of the precipitated phases. These innovative structures not only optimize material properties at the microscopic level but also achieve higher strength and toughness by fine-tuning the phase interfaces and defect distributions.

Using SLM technology, Mu *et al.* successfully combined a high-density dislocation structure with a high-volume fraction of malleable nanoprecipitates in the $Fe_{28.0}Co_{29.5}Ni_{27.5}Al_{8.5}Ti_{6.5}$ MPEA[96]. As depicted in Figure 8, this material presents a novel dislocation-precipitate skeleton structure embedded with high-density malleable nanoprecipitates, exhibiting an impressive tensile strength of approximately 1.8 GPa and a maximum elongation of about 16%. The ultra-high strength primarily results from the synergistic strengthening effects of dislocations and precipitates, while the notable ductility is attributed to the evolution of multiple stacking fault structures.

Moreover, the dislocation skeleton slows the movement of dislocations during deformation without completely obstructing their motion, thus maintaining structural stability and preventing premature failure due to boundary stress concentrations. This balance between strength and ductility illustrates the potential of tailored microstructures in enhancing the performance of MPEAs. This greatly benefits the overall performance of the material, though specific material systems must be considered.

Lamellar structure

Another common structure observed in AM is the lamellar structure, which consists of alternating layers of different phases, providing unique mechanical advantages.

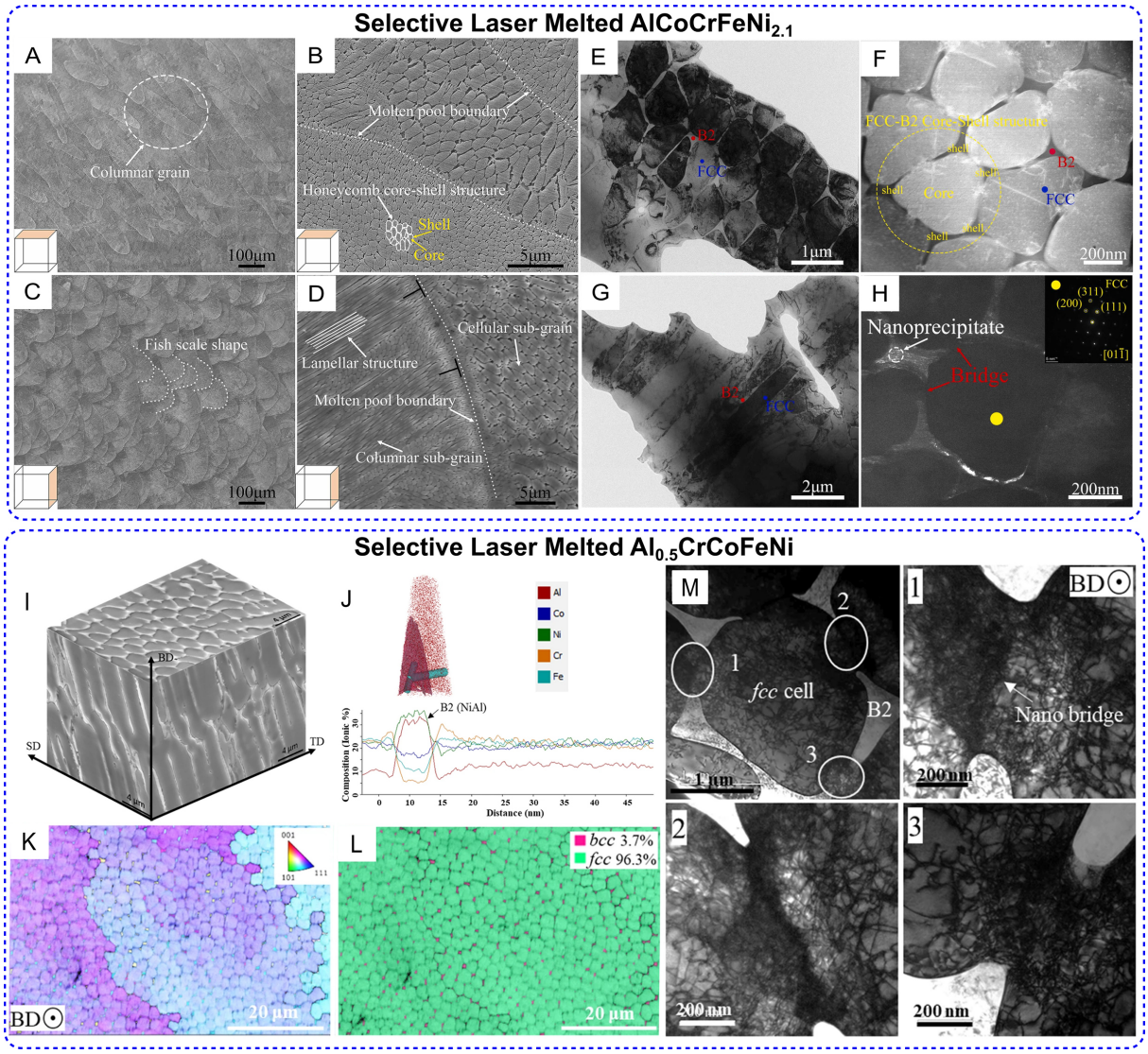

Figure 7. Core-shell structures created by LAM techniques: (A and B) Microstructure perpendicular to building direction (BD) of the SLM-AlCoCrFeNi$_{2.1}$; (C and D) Microstructure parallel to BD; (E and F) The micrograph of core-shell structure; (G) The micrograph of lamellar structure; (H) The micrograph of nanoprecipitate and bridge[94]. (I) pseudo-3D microstructure of SLM-Al$_{0.5}$CrCoFeNi; (J) Quantitative compositional analysis by atom probe tomography (APT) shows the distribution of different elements in the face-centered cubic cells and B2 phase on the boundaries; (K) IPF map showing the near-uniform crystallographic orientation in different grains; (L) the corresponding phase map showing the consistent distribution of the B2 (body-centered cubic) phase on the face-centered cubic cell boundaries; (M) TEM images show the morphology of the B2 phase on the boundaries, with the magnified images from locations 1, 2, and 3 showing the nanometer-scale bridges (nano-bridges), where high-density dislocations are observed[95].

For instance, Ren *et al.* prepared a dual-phase AlCoCrFeNi$_{2.1}$ MPEA using SLM, achieving remarkable mechanical properties with a yield strength of up to 1.3 GPa and a uniform elongation of 14%[35]. This exceptional performance is attributed to its unique layered nanoscale microstructure, which features alternating nanoscale face-centered cubic and body-centered cubic phases, along with semi-coherent interfaces and chemical segregation of components at the nanometer scale [Figure 9A-D]. The high strength results from the nanolayered structure and elevated print-induced fault density, while significant plastic deformation is facilitated by the high strain-hardening capacity of the body-centered cubic phase. Additionally, nanoscale chemical segregation, varying orientations in adjacent regions, and continuous strain gradients further enhance the strain hardening of the body-centered cubic phase.

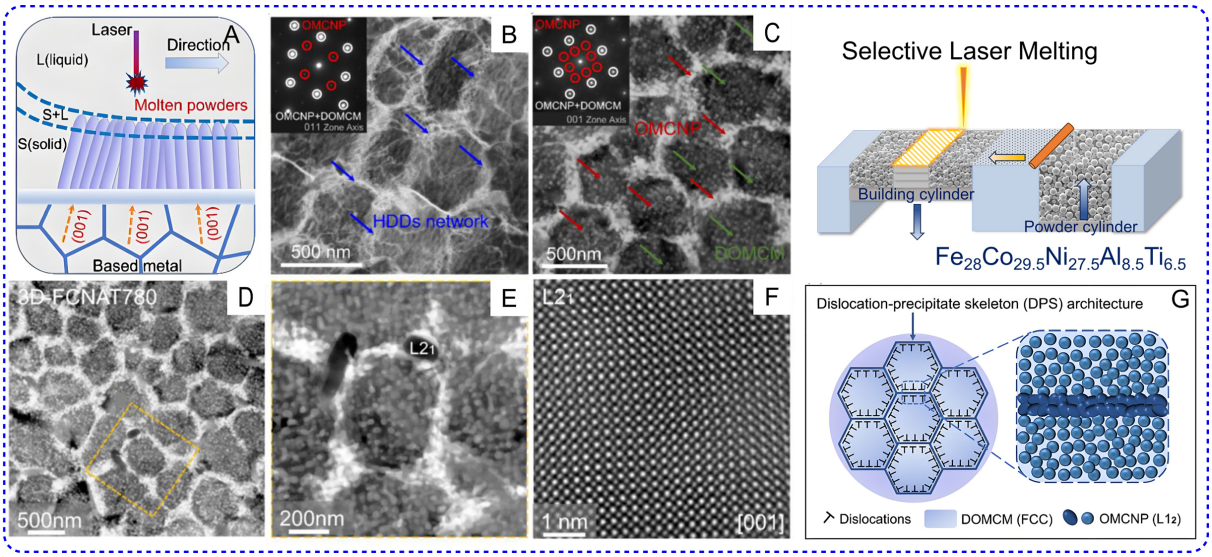

Figure 8. Skeleton architecture created by LAM techniques: (A) Solidification process of SLM-$Fe_{28.0}Co_{29.5}Ni_{27.5}Al_{8.5}Ti_{6.5}$; (B) Bright field (BF) scanning transmission electron microscopy (STEM) image of prepared showing the high-density dislocations network with the selected area electron diffraction (SAED) pattern from (011) zone axis showing the corresponding microstructure; (C) BF STEM image showing the sub-grain architectures consist of the face-centered cubic disordered multicomponent matrix (DOMCM) phase and $L1_2$ ordered multicomponent nanoprecipitate (OMCNP) phase, with SAED pattern from (001) zone axis showing the corresponding microstructure; (D) BF STEM image showing the sub-grains composed of face-centered cubic , $L1_2$ and a small amount of $L2_1$ phase; (E) The enlarged view of the local sub-grain feature area. (F) The high-resolution high-angle annular dark-field imaging (HADDF) -STEM image of $L2_1$; (G) The dislocation-precipitate skeleton architecture[96].

Another example is that Huang *et al.* utilized LDD to fabricate the $AlCoCrFeNi_{2.1}$ [Figure 9E-J] MPEA[97]. Similarly, the MPEA produced by LDD exhibits a face-centered cubic/body-centered cubic dual-phase eutectic microstructure. This fine and uniform eutectic structure significantly improves the strain hardening and dislocation accumulation capacity of the EMPEA, thereby enhancing its mechanical properties. The LDD process capitalizes on the high cooling rates and eutectic characteristics to form a refined microstructure, resulting in excellent mechanical performance.

In addition, the precise control offered by LAM allows different materials to be combined for achieving artificial lamellar structures. For example, Sun *et al.* used LDD to create a multilayer heterostructured MPEA alloy. This alloy consists of alternating entropy-intermediate alloys of CoCrNi and $(CoCrNi)_{86}Al_7Ti_7$[98] [Figure 9K-N]. After appropriate heat treatment, the heterostructure alloy achieves an ultimate tensile strength of over 1 GPa and an elongation at break of 50.6%. These results are much higher than those reported for medium or high entropy alloys in other studies. The improved performance is mainly due to the formation of a nanoscale $L1_2$ phase in the CoCrNi layer during heat treatment. Additionally, the gradient transition of the eutectoid in the $(CoCrNi)_{86}Al_7Ti_7$ layer helps prevent the formation of brittle nanoscale lamellar structures. The composition gradient and low strain gradient at the heterogeneous interface work together to enhance both strength and toughness.

Nano precipitates

In the heterostructures prepared using laser-based technology, precipitates play a crucial role especially at nanoscale. These nano precipitates can be uniformly distributed within the matrix by precisely controlling laser parameters and material compositions, significantly enhancing the mechanical properties and corrosion resistance of the materials. The formation mechanism of nano precipitates involves phase separation and the precipitation of solid solutions, resulting in superior properties especially in the

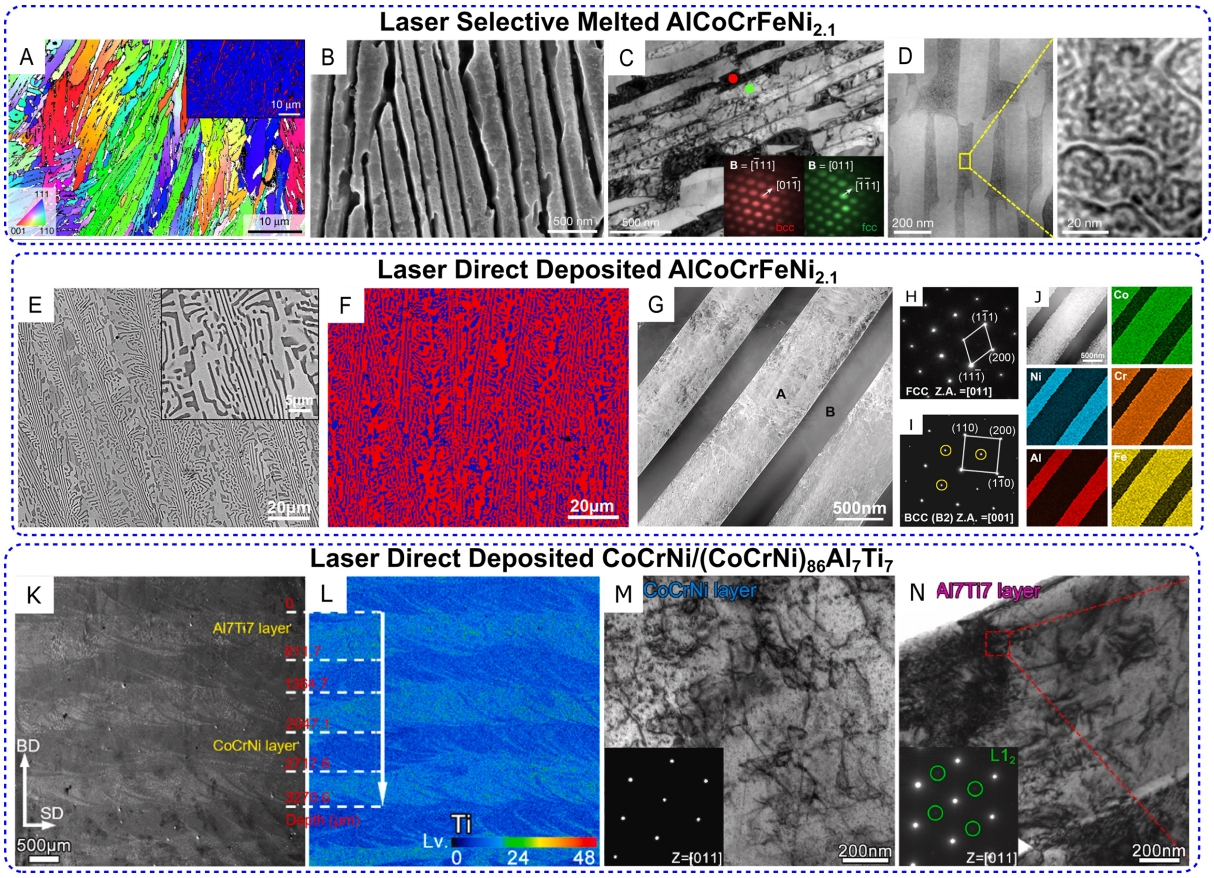

Figure 9. Lamellar structures created by LAM techniques: (A) IPF map of SLM- $AlCoCrFeNi_{2.1}$, showing a magnified local region; (B) Secondary electron micrograph of the nanolamellar structure; (C) Bright-field TEM image of the body-centered cubic and face-centered cubic nanolamellae with PED patterns; (D) HAADF-STEM image showing the modulated nanostructures within body-centered cubic lamellae[35]. (E) BSE images of LDD-$AlCoCrFeNi_{2.1}$; (F) The phases distribution; (G) TEM image of sample; (H) The corresponding SAED pattern taken from the A zone of (G); (I) The corresponding SAED pattern taken from the B zone of (G); (J) The elemental distributions of the frames in (G)[97]. (K) SEM image of LDD-CoCrNi/$(CoCrNi)_{86}Al_7Ti_7$ on building direction-sectional direction (BD-SD) plane; (L) EPMA mapping; (M and N) Typical BF-TEM images of CoCrNi layer and $(CoCrNi)_{86}Al_7Ti_7$ (denoted as Al_7Ti_7) layer in the sample, respectively[98].

enhancement of strength. For instance, Mu *et al.* utilized SLM to prepare $Fe_{28}Co_{29}Ni_{27.5}Al_{8.5}Ti_{6.5}$ MPEA samples[99]. Through short aging heat treatment, they successfully retained a high-density dislocation structure while simultaneously inducing the formation of duplex ordered nanoscale precipitates ($L1_2$ and $L2_1$), as shown in Figure 10A-D. These nanoprecipitates are uniformly distributed within the subgrain boundaries and grains, significantly improving the strength and ductility. The combination of these nanoprecipitates and the *in-situ* dislocation network promotes the strain hardening mechanism, resulting in an impressive ultra-high strength of 1,430 MPa and an elongation of nearly 16%.

In another study, Miao *et al.* enhanced the surface properties of $AlCoCrFeNi_{2.1}$ MPEA through LSR and aging heat treatment[100]. After LSR, the surface microhardness of the alloy increases by 59%, while the average friction coefficient and wear rate decrease by 26% and 68%, respectively. This improvement is attributed to the reduction in the lamellar spacing of the face-centered cubic and body-centered cubic (B2) phases and the formation of consistent nanoprecipitates within both phases as depicted in Figure 10E.

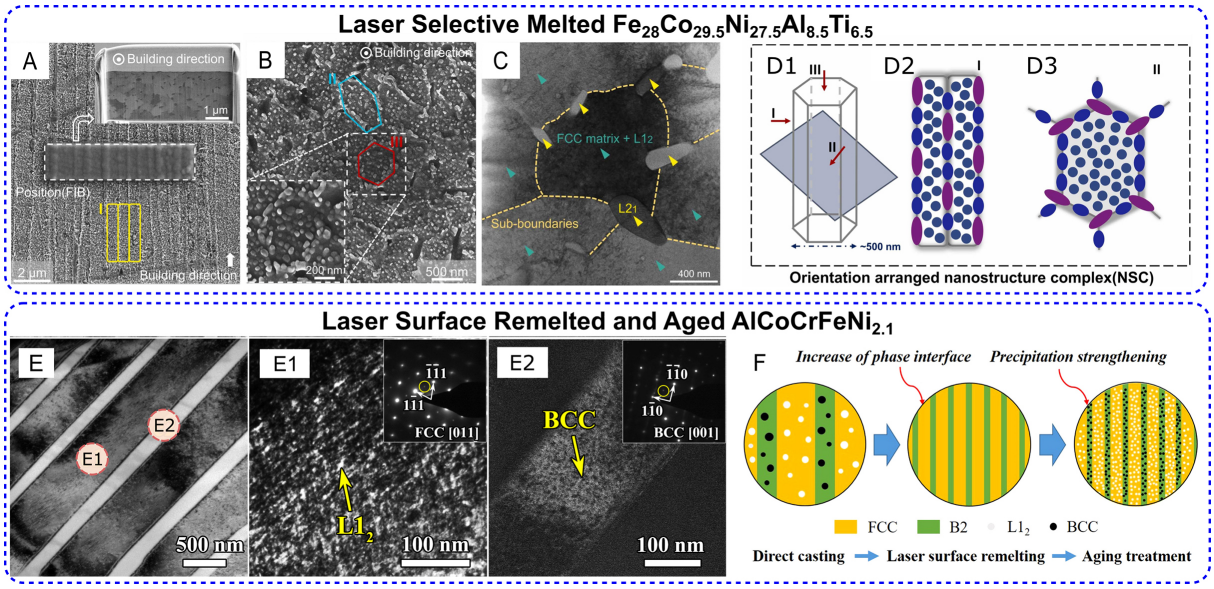

Figure 10. Heterostructures with nano precipitates created by LAM and LST techniques: (A) SEM image showing the orientation arranged nanostructure complex parallel to the BD of SLM-$Fe_{28}Co_{29}Ni_{27.5}Al_{8.5}Ti_{6.5}$; (B) SEM image showing the multiple nanoprecipitates manipulation; (C) TEM image showing the $L1_2$, $L2_1$, and face-centered cubic matrix phases; (D) Schematic illustration of the orientation arranged nanostructure complex composed of multiple nanoprecipitates manipulation and *in-situ* dislocation network[99]. (E) BF TEM images of the LSR & aged $AlCoCrFeNi_{2.1}$ MPEAs; Dark field (DF) TEM images of the face-centered cubic phase (E1) and B2 phase (E2) from the superlattice spot from their selected area diffraction patters (SADPs) shown in the inset. (F) Schematic diagrams of the surface-strengthening process[100].

The remelting process significantly refines the alloy's microstructure, promoting the formation of nanoprecipitates in both the face-centered cubic and body-centered cubic phases [Figure 10F]. Subsequent aging treatment at 600 °C enhances the quantity and distribution of these precipitates, further enhancing the alloy's hardness and wear resistance. Although rapid cooling during laser remelting initially inhibits precipitate formation, the subsequent heat treatment allows for an even distribution and increased strength of the precipitates. The presence of these nanoprecipitates increases the phase interfaces, enhancing the mechanical properties of the alloy, particularly during plastic deformation.

These findings highlight the importance of nanoprecipitates in improving the properties of MPEAs and offer valuable insights for optimizing alloy microstructures at nanoscale.

Hierarchically heterogeneous structure

Building on the previously discussed concepts, it is evident that the rapid cooling characteristics of laser processing technology, combined with the inherent complexity of MPEA systems, often result in a hierarchically heterogeneous microstructure. This type of structure incorporates multiple phases and forms, enhancing material properties. Actually, some of the aforementioned cases belong to the category of hierarchically heterogeneous structure, such as dual-phase or multi-phase with gradient distribution of composition or grain sizes, along with nanoparticipates embedded in lamellar structures. Herein, more typical hierarchically heterogeneous structures will be introduced to broaden our horizons.

For example, Luo *et al.* investigated a $TiZrHfTaNb_{0.5}$ MPEA and highlighted this phenomenon[101]. The as-cast MPEA exhibits a single body-centered cubic solid solution phase with an average grain size of approximately 115 μm. However, after LSR treatment, a GNS layer about 100 μm thick formed on the surface, showcasing a gradual refinement of grain size with decreasing depth, as illustrated in Figure 11A-J.

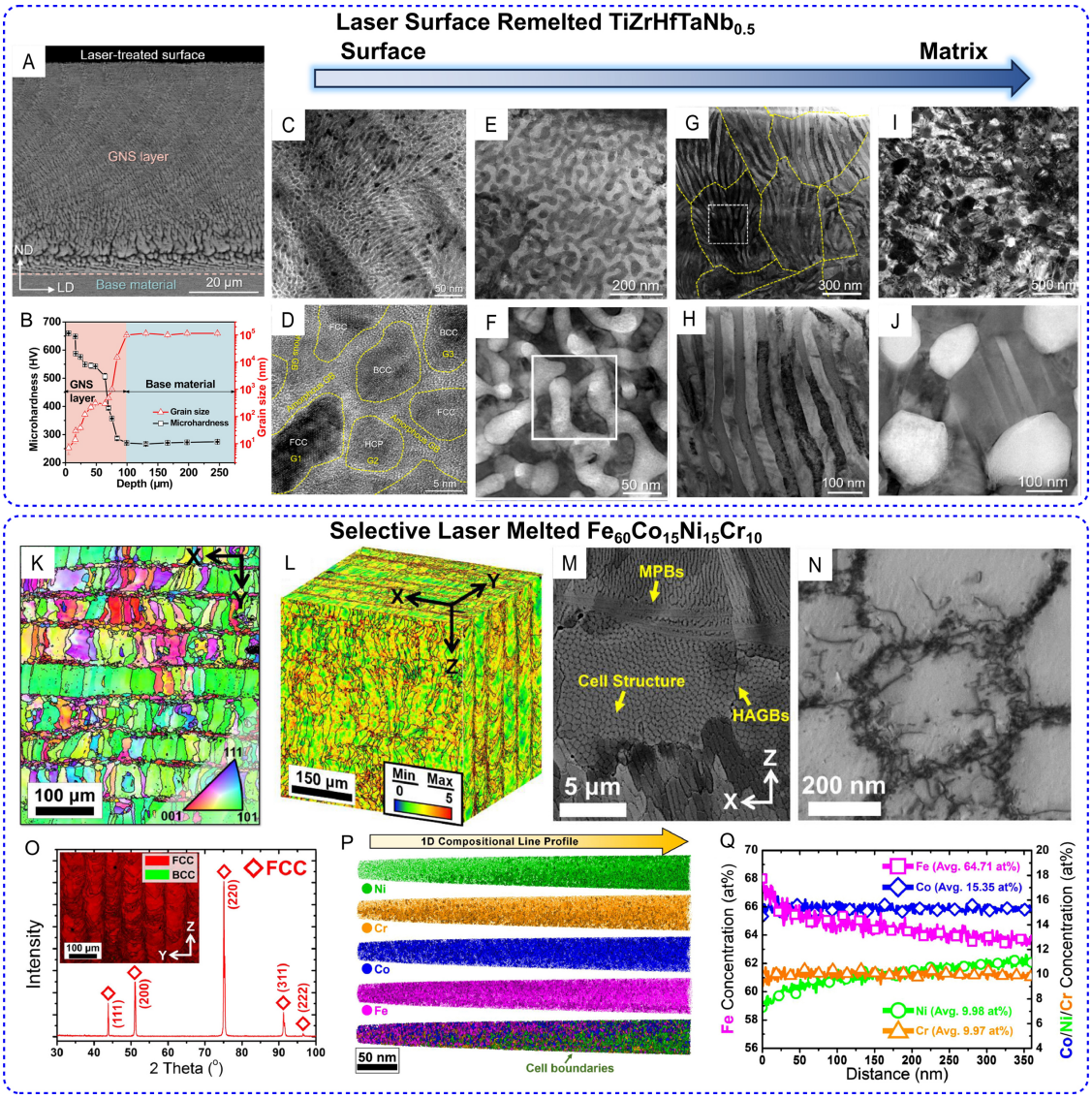

Figure 11. Hierarchically heterogeneous structures created by LAM and LST techniques: (A) SEM image showing the morphology along the depth direction of the LSR-TiZrHfTaNb$_{0.5}$; (B) Variations of grain size and microhardness along the depth away from the topmost surface; TEM characterization of crystalline-amorphous nanostructured surface layer (C and D) and at a depth of 10-20 μm (E and F); 20-40 μm (G and H) and 40-60 μm (I and J) below the surface[101]. (K) IPF map of building plane of the SLM-$Fe_{60}Co_{15}Ni_{15}Cr_{10}$; (L) The pseudo-3D EBSD KAM maps; (M) SEM. (N) STEM image of solidification cells; (O) XRD pattern with inset showing EBSD phase maps on the plane normal to the scan direction; (P) 3D reconstructed element distributions near the cell boundaries by APT analysis; (Q) 1D concentration profiles of the 3D element distribution in the APT maps[102].

Within this GNS layer, remarkable microstructural evolution occurred, including the formation of ultrafine grains, precipitated nanostructures, and a unique crystalline-amorphous heterostructure at the topmost layer.

The development of this complex microstructural architecture is attributed to phase decomposition-mediated gradient refinement mechanisms. The high-energy LSR process melts the outermost surface, creating an amorphous state. Subsequently, rapid and gradient cooling rate during solidification leads to partial crystallization, resulting in the distinctive crystalline-amorphous nanostructure.

Further analysis revealed that compositional segregation and phase transformations significantly influence the evolution of the GNS layer. The initial body-centered cubic solid solution matrix underwent various phase decompositions, resulting in TiTaNb-rich body-centered cubic, ZrHf-rich body-centered cubic, ZrHf-rich face-centered cubic, and minor hexagonal close-packed phases, with their distribution and grain sizes varying along the depth. These compositional and structural changes are closely related to the gradient thermal conditions - temperature and cooling rate - experienced during the LSR process.

Additionally, Park *et al.* demonstrated the excellent mechanical properties of an iron-based medium-entropy alloy $Fe_{60}Co_{15}Ni_{15}Cr_{10}$ fabricated using SLM[102]. The SLM process introduces spatial and compositional heterogeneity into the alloy, characterized by anisotropic grain morphology, a honeycomb submicroscopic cell structure, and compositional segregation at cell boundaries [Figure 11K-Q]. The size and morphology of grains differ significantly in various directions, while the honeycomb cell structure contributes to a unique microstructure that enhances both strength and toughness.

Significant compositional segregation, particularly at cell boundaries, results in variations in chemical composition across different regions. This segregation reduces the stability of the face-centered cubic phase and promotes strain-induced martensitic transition [transformation-induced plasticity (TRIP)], generating a high-density dislocation network that significantly strengthens the material's yield strength. These unique microstructural characteristics not only enhance the yield strength of the alloy but also improve its ductility through strain-induced phase transformation strengthening.

These findings illustrate that remarkable microstructural control is achievable in hierarchically heterogeneous alloys through advanced laser-based techniques. The intricate interplay between grain refinement, phase transformations, nanoprecipitates, and the formation of crystalline-amorphous heterostructures are expected to contribute to better mechanical performance, paving the way for the development of advanced structural materials with superior properties.

MECHANICAL AND FUNCTIONAL PROPERTIES

In the previous section, we have elaborated on various methods for fabricating heterostructured MPEAs and some typical microstructures obtained. These distinctive material microstructures not only exhibit unique characteristics during the production process but also contribute effectively to approaching remarkable mechanical properties and damage tolerance[57].

Strength-ductility synergy

For conventional metals and alloys, strength and ductility are mutually exclusive, as illustrated by the curve in Figure 12. Overcoming this strength-ductility trade-off is a major challenge in metallic materials[57,128]. Reducing the grain size to nanoscale is an effective strategy to increase the strength, as grain boundaries can effectively block dislocation motion. However, this grain refinement also leads to a significant loss in ductility due to the constraint of plastic deformation mechanisms within small grains. Heterostructured materials, however, provide a novel pathway to address this dilemma[129,130]. Extensive experimental studies have demonstrated that these structured materials possess an exceptional combination of mechanical properties, often overcoming traditional trade-offs. As illustrated in Figure 12, various microstructural designs created by laser-based techniques demonstrate exceptional mechanical properties that often exceed the traditional limitations seen in homogeneous MPEAs. The unique configurations of heterostructured materials represented by different marks illustrate that the laser-processed variants can achieve higher yield strengths without a proportional loss in elongation, in contrast to conventional homogeneous MPEAs (depicted as purple squares) that tend to cluster in the lower strength and ductility regions. Independent

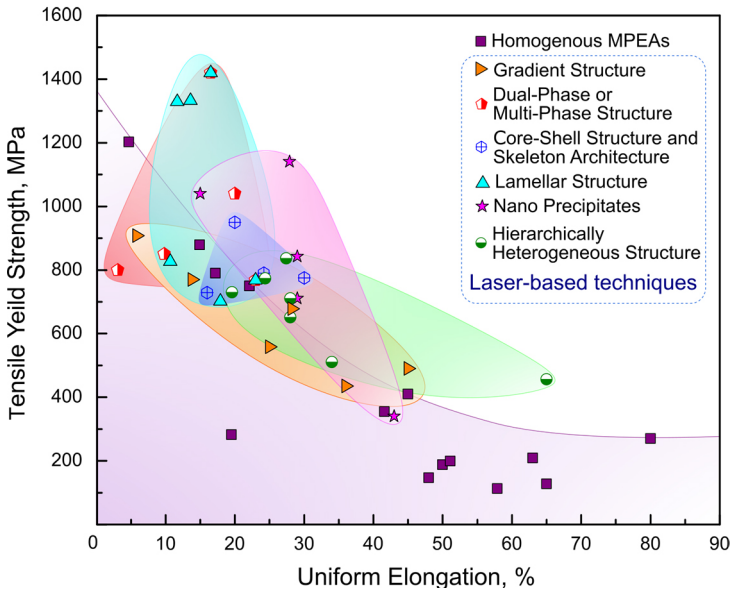

Figure 12. Normalized yield strength versus uniform elongation of homogeneous and laser-processed heterostructured MPEAs[28,35,86,88,90,95,97-100,102,103-127].

heterostructures, such as lamellar configurations or nanoprecipitates, demonstrate significant benefits for achieving strength enhancements but less improvement in ductility. However, core-shell structures and hierarchically heterogeneous structures provide notable advantages in plasticity retention. Consequently, the combination of multiple hetrostructures may inspire us more to solve the challenge of strength-ductility trade-offs.

Here are some typical examples of how specific heterostructures affect their performance. Recent investigations by Zhang *et al.* have revealed how inverse gradient-grained CoCrFeMnNi high-entropy alloys effectively transcend the conventional trade-off between strength and ductility[88]. Through a novel processing method involving cold rolling followed by laser surface heat treatment, these alloys exhibit a unique gradient in grain sizes, which transitions from smaller and harder grains at the core to larger and softer grains at the surface. This gradation aligns closely with their microhardness profiles, optimizing the material's mechanical properties.

This structural gradient not only enhances strength via HDI strengthening and strain hardening but also preserves ductility through the formation of high-order hierarchical nanotwins that interact synergistically with dislocations. The heterostructured samples outperform conventional homogeneous samples in tensile tests, exhibiting high yield strength (approximately 678 MPa), tensile strength (approximately 830 MPa), and notable ductility (about 28.2%).

The inverse gradient grain structure plays a pivotal role during tensile testing by promoting the formation of geometrically necessary dislocations and deformation twins. These features accommodate the strain gradient, significantly improving mechanical performance. Additionally, the interfaces between coarse and fine grains serve as sites for accumulating high densities of dislocations, generating back stresses that restrict dislocation movement in the softer regions, thus contributing to enhanced yield strength and further work hardening.

Building on these foundational insights, Kim *et al.* have further expanded the application of inverse-gradient structures in CoCrFeMnNi MPEAs through a similar approach[123]. Their method involved cold rolling followed by LSR on both sides of the alloy sheets, resulting in a multi-scale heterogeneous microstructure. This structure features a gradient, transitioning from coarse grains at the surface to fine grains in the middle, with partially recrystallized grains at the core, resembling Figure 4E. The inverse gradient heterostructured samples exhibit superior tensile properties, with a yield strength of approximately 907.6 MPa and an ultimate tensile strength of around 949.4 MPa. Unlike the previously mentioned outer-soft and inner-hard structures, these inverse gradient heterostructured samples demonstrate excellent bendability, as the outer coarse-grained region prevents crack initiation. Although the presence of a coarse-grained area may reduce tensile performance compared to other gradient materials, it still outperforms homogeneous materials, and the decrease in strength differences between neighboring domains mitigates damage evolution. Thus, the produced heterogeneous HEAs exhibit superior tensile and forming properties.

Building upon the previously discussed strength-ductility trade-off, heterostructured materials have emerged as a promising solution to enhance work hardening capacity as well[131,132]. This section delves into the work hardening phenomena in heterostructured materials, revealing their unique micro-mechanisms and macroscopic manifestations.

Fu *et al.* investigated the strain distribution and work hardening behavior of $CoCrFeNiMn_{0.75}Cu_{0.25}$ MPEA treated by LSP under uniaxial tensile loading, and the gradient structures formed inside the component are similar to those illustrated in Figure 3[122]. It was found that the yield strength of the sample after four LSPs was increased by 1.5 times, and the elongation reached 40%. LSP treatment significantly improves the strain hardening ability of MPEA, which is mainly achieved by the combination of dislocation hardening and mechanical twins. The refined nanograins and nanotwins in the gradient structure form a dense shear band at the low strain stage and remain stable throughout the plastic deformation process, thus accommodating the major tensile strain and improving the overall strain hardening effect. In addition, the multi-axial strain transformation in the graded structural materials promotes the activation of multiple slip systems, further enhancing dislocation hardening. Consequently, this results in the enhancement of both strength and hardness while maintaining good plasticity in the interior, achieving a synergistic growth of strength and ductility. It should be noted that, for materials with internal porosity or cracks, cracks typically initiate at the weakest points surrounded by tensile stress during tensile tests, subsequently propagating until fracture occurs. However, shock waves influence the target during the LSP process, compressing porosity and transforming the stress state around these regions from tensile to compressive, significantly improving tensile performance.

Recent advancements by Zhu *et al.* have demonstrated the significant work hardening capacity in an interstitial solute-strengthened MPEA, $Fe_{49.5}Mn_{30}Co_{10}Cr_{10}C_{0.5}$, fabricated via SLM[115]. The as-built MPEA exhibits a hierarchically heterogeneous microstructure, which is critical for its enhanced mechanical properties. The alloy boasts a high yield strength of approximately 710 MPa and an ultimate tensile strength of around 1 GPa, combined with a notable uniform elongation of about 28%, showcasing exceptional strength-ductility synergy.

The substantial work hardening in this MPEA is attributed to deformation mechanisms such as dislocation slip, deformation twinning, and phase transformation. Initially, high dislocation density within cellular structures leads to significant dislocation storage. As deformation progresses, planar slip bands and stacking faults enhance work hardening. The formation of deformation twins and deformation-induced hexagonal close-packed phases further accommodate deformation and act as strong barriers to dislocation movement,

maintaining a high work hardening rate. The hierarchically heterogeneous microstructure, spanning several length scales, plays a pivotal role in mechanical performance. This microstructural design enhances back stress and HDI hardening, promoting homogeneous deformation and resulting in superior mechanical properties.

Similarly, Fe-based MPEAs were fabricated using SLM by Park *et al.*, where the SLM process introduces a microstructure with spatial and compositional heterogeneity[102]. High dislocation density is the main contributing factor to the high strength. Solute segregation induced by SLM lowers the phase stability of the matrix and promotes strain-induced martensitic transformation, as shown in Figure 13A-G. The synergy of high dislocation density and strain-induced martensitic transformation enhances the alloy's strength and ductility.

In addition to experimental studies, simulations have been conducted to uncover the underlying mechanisms responsible for the property enhancements in heterostructured MPEAs. For example, Peng *et al.* conducted molecular dynamic simulations to investigate the rate-dependent deformation behavior and multistage strain hardening mechanisms of GNS MPEAs[133] [Figure 13H-P]. Their simulations show that below a strain rate of 10^8 s^{-1}, dislocation slip and deformation twinning are the main mechanisms. At a strain rate of 10^9 s^{-1}, deformation twinning coexists with phase transformations, while at a strain rate of 10^{10} s^{-1}, phase transformations dominate. Additionally, edge dislocations, rather than screw dislocations, enhance the materials' strength. A microstructure-based constitutive model using a single parameter set is developed from the atomic simulations, accurately predicting the mechanical properties of MPEAs across various strain rates. Moreover, some structures can also be effectively produced through laser-based techniques, as demonstrated in Figure 13H. However, further investigations are still needed for specific systems prepared using different laser techniques. Challenges remain, particularly in obtaining precise parameters and in the complexity of modeling varying microstructures associated with laser-fabricated MPEAs.

These studies highlight a paradigm shift in understanding work hardening mechanisms in hetero-structured materials. Structural heterogeneity across multiple scales - from atomic to microscopic - creates a complex landscape for strain accommodation. This approach optimizes dislocation-microstructure interactions through gradient structures, nanotwins, multi-phases, and nanoprecipitates, leading to superior mechanical performance.

Fatigue resistance

Fatigue resistance is another critical consideration in the design and application of structural materials, as it directly influences the operational lifetime and safety of components subjected to cyclic loading. Interestingly, the unique microstructural architectures of heterostructure materials have been shown to significantly enhance the fatigue life of metallic systems[134].

The study by Kim *et al.* highlights the exceptional capabilities of SLM in crafting CoCrFeMnNi MPEAs with refined microstructural features that substantially boost their high-cycle fatigue resistance[117]. Unlike conventional manufacturing processes, SLM enables the precise control of microstructural evolution during the fabrication, leading to the formation of heterostructures characterized by nanosized oxide dispersions within a heterostructured metallic matrix. These oxides, formed *in-situ* during the SLM process, are strategically located at substructural and grain boundaries, serving as crucial barriers to dislocation movement and crack propagation.

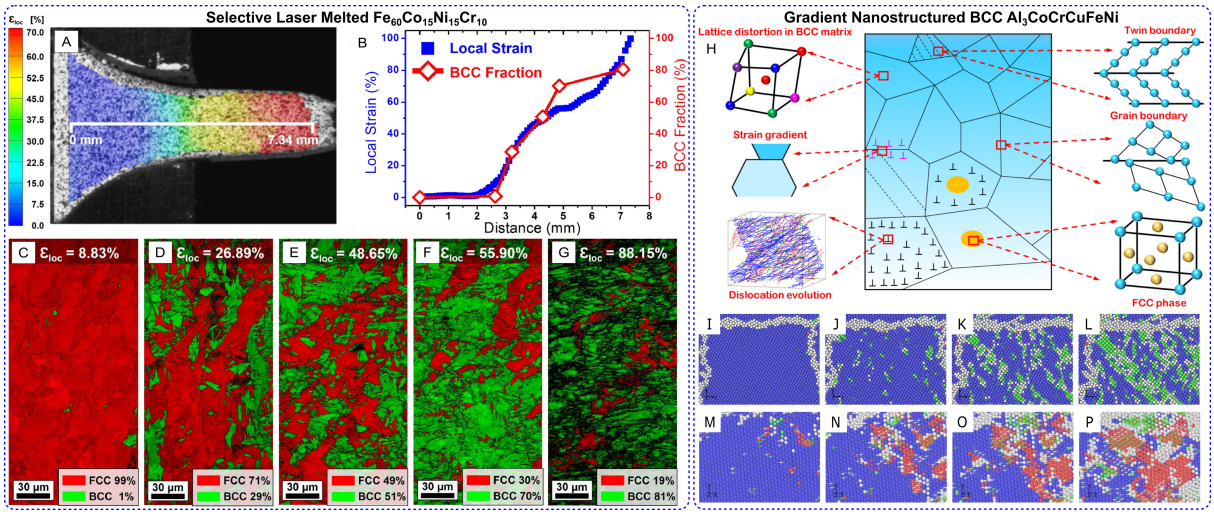

Figure 13. (A) Local strain distribution maps on the tensile-fractured SLM-$Fe_{60}Co_{15}Ni_{15}Cr_{10}$ obtained by the DIC analysis; (B) Evolutions of local strain and BCC phase fraction measured by DIC and EBSD analysis; (C-G) EBSD phase maps showing the deformation-induced martensitic transformation as a function of plastic deformation[102]. (H) The schematic illustration of heterostructured $Al_3CoCrCuFeNi$ MPEA; The simulated BCC to FCC phase-transformation process with the increased strain: 2% (I), 5.5% (J), 8% (K), and 10% (L) at the strain rate of 1×10^{10} s^{-1}; The simulated BCC to HCP phase-transformation process with the increased strain: 5% (M), 7% (N), 8% (O), and 10% (P) at the strain rate of 1×10^{10} s^{-1}[133].

In this heterostructured alloy, the fatigue limit is found to be significantly elevated at 570 MPa, a stark contrast to the 280 MPa observed in traditionally manufactured MPEAs [Figure 14A]. This improvement is not merely a function of enhanced material strength but is deeply rooted in the synergy between the nano-dispersed oxides and the underlying dislocation networks formed during the rapid solidification inherent to SLM. Additionally, the presence of deformation twins, induced under cyclic loading, plays a vital role in enhancing the material's ductility and in blunting potential crack tips, further impeding the fatigue crack propagation.

Furthermore, the heterogeneous grain structure and dislocation networks typical of SLM-built materials contribute additional mechanical integrity by distributing stress more evenly across the material, thereby reducing the stress concentration at any single point. The structural complexity made by the SLM technique exemplifies the potential of heterostructured designs in pushing the boundaries of what is achievable in terms of mechanical performance and durability of MPEAs under cyclic loading conditions.

As the temperature changes, the performance sometimes might be largely different. Jin *et al.* examined the fatigue behavior of CoCrFeMnNi MPEAs fabricated by SLM across a temperature range of 22-600 °C[135]. The study found that the alloy exhibits transient cyclic hardening followed by cyclic softening at all temperatures tested [Figure 14B]. The high dislocation density, resulting from the manufacturing process, effectively absorbs most applied strain, leading to initial hardening.

However, as temperature increases, the reduction in dislocation density results in decreased cyclic strength and related properties, such as yield strength and friction stress. Notably, the transition from transgranular to intergranular fracture morphology at elevated temperatures significantly influences fatigue life, highlighting the critical role of microstructural stability under varying conditions.

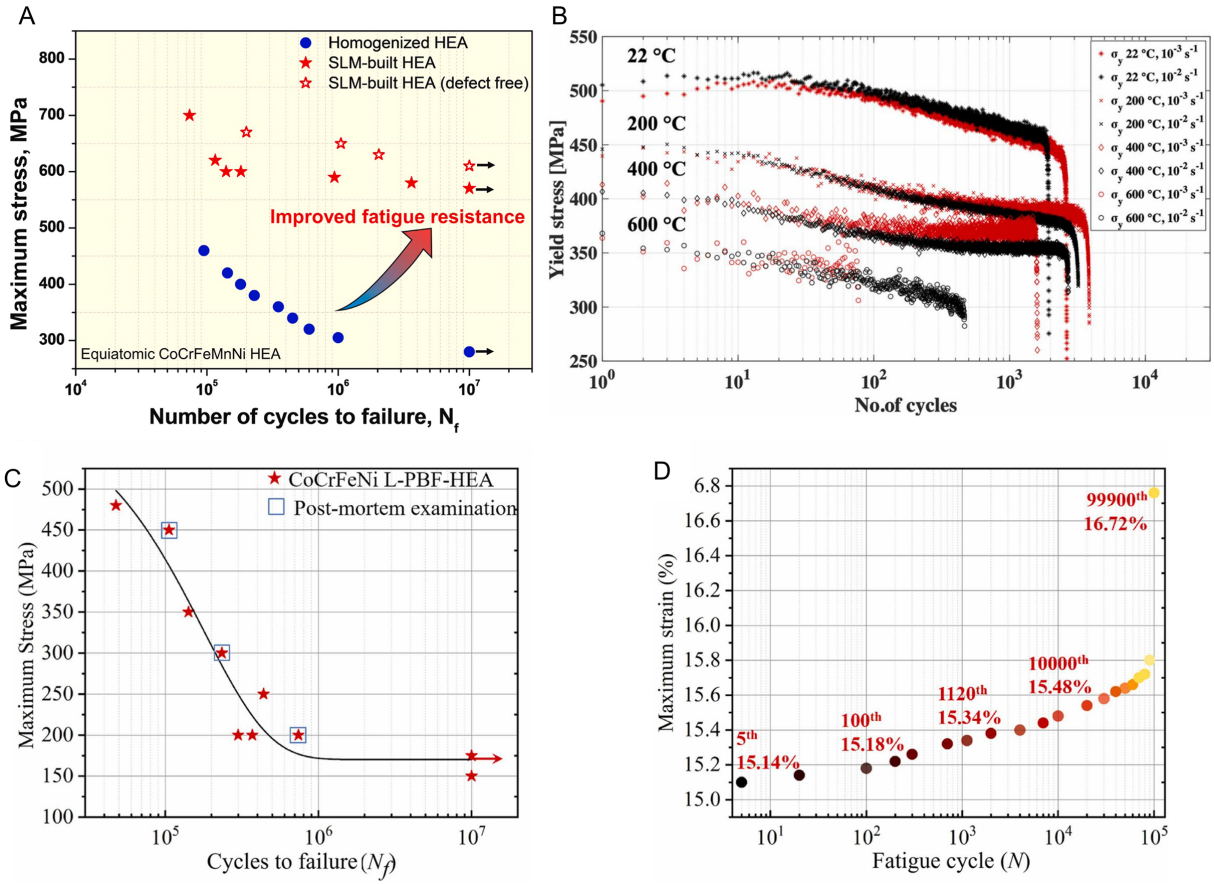

Figure 14. Fatigue resistance of MPEAs prepared by laser-based techniques: (A) S-N curves of SLM-CoCrFeMnNi[117]. (B) Evolution of the yield stress at an offset strain of 0.01% after cyclic loading at different temperatures and strain rates of SLM-CoCrFeMnNi[135]. High-cycle fatigue of SLM-CoCrFeNi: (C) S-N curve with the specimens used for the post-mortem examination indicated by the square box; (D) A plot of the measured maximum strain vs. fatigue cycles for the specimen tested under the maximum stress of σ_{max} = 450 MPa with a fatigue life of $N_f = 1.06 \times 10^5$[136].

Chen *et al.* explored the microstructural evolution of a CoCrFeNi MPEA manufactured using SLM under high-cycle fatigue conditions[136]. In their tests, deformation twinning is observed at a maximum stress of 450 MPa, while no twinning occurs at lower stress levels [Figure 14C and D]. This twinning leads to cyclic softening, accompanied by an increase in hardness, demonstrating the complex interplay between microstructure and fatigue behavior. The evolution of stacking faults and a maze-like dislocation structure within the alloy is another critical mechanism influencing fatigue performance. These features contribute to the alloy's ability to accommodate strain and enhance resistance to crack initiation.

Those enhanced fatigue resistance observed in these heterostructured MPEAs can be attributed to several key mechanisms: Special microstructural features such as the presence of nanosized oxide dispersions and a heterogeneous grain structure improve resistance to crack initiation and propagation; The intricate dislocation networks formed during processing allow for effective energy dissipation during cyclic loading; The generation of deformation twins under stress not only improves ductility but also serves as a dynamic strengthening mechanism and the stress distribution; The heterogeneous microstructure facilitates uniform stress distribution, reducing localized stress concentrations that can lead to premature failure.

Currently, relatively few studies have explored the fatigue properties of heterostructured MPEAs. Understanding the underlying mechanisms is essential for optimizing alloy design and ensuring the longevity and safety of structural components in demanding applications, especially in extreme environments.

Wear resistance

Wear and friction significantly influence the service life and reliability of industrial components. With the advances in mechanical properties, heterostructured metallic materials have also shown substantial improvements in wear and friction resistance. The unique microstructural features and tailored interfaces play a vital role in modulating the tribological performance of these advanced MPEAs as well.

A notable example of this approach is demonstrated in a heterostructured TiZrHfTaNb MPEA fabricated via LSR[93]. Luo *et al.* created a ~100 μm-thick layer with grain sizes reduced from ~200 μm to ~8 nm at the surface, increasing microhardness from ~240 to ~650 HV - a 2.7-fold improvement[93]. This refinement also leads to phase decomposition and a depth-dependent phase distribution, significantly enhancing wear resistance by reducing wear rates by an order of magnitude compared to the base alloy. The researchers attributed this remarkable enhancement in tribological performance to the synergistic effects of the decomposed multi-phases and the gradient nanostructures, which collectively mitigated various wear mechanisms, including abrasive, oxidative, and adhesive wear. For systems prone to phase decomposition or the formation of amorphous structures, the selected LSR technique can induce a gradient distribution of solidification and cooling rates along the depth direction. This means the LSR process effectively melts the outermost surface region (resulting in an amorphous state), which will also experience the highest cooling rates. Consequently, crystallization during the subsequent solidification process may be only partially completed, leading to the formation of a crystalline-amorphous nanostructure. Additionally, rapid solidification processes (lasting only a few tens of milliseconds) can significantly inhibit atomic diffusion for element homogenization and the growth of newly formed second phases, particularly for sluggish elements. The rapid gradient cooling rates during the LSR process result in the growth of gradient grains in the newly formed phases, ultimately leading to the formation of a GNS layer[93,101].

Another common approach is introducing new components for better surface properties; for instance, the recent research by Guan *et al.* introduces an innovative W/FeCoCrNi-based MPEA gradient coating, developed through LC[92]. This study highlights the development of a dual-phase structure with Laves and face-centered cubic phases, engineered via the two-way diffusion behavior of FeCoCrNi and W elements during solidification. The resulting microstructure, characterized by a strategic hardness gradient and phase distribution, optimizes both hardness and plasticity. The hard Laves phase provides excellent wear resistance, while the ductile face-centered cubic phase maintains the coating's plastic deformation capabilities, crucial for operational toughness.

Moreover, the coating's robust wear resistance is notably enhanced by a protective oxide film formed during the wear process. At elevated temperatures, the synergistic interaction between the hard and ductile phases effectively reduces stress concentrations during friction, optimizing the balance between hardness and ductility, essential for maintaining structural integrity under extreme conditions. Additionally, the transitional eutectic layer between these phases acts as a stress buffer, further enhancing the coating's durability. Table 1 summarizes the wear characteristics of some homogenous and laser-fabricated MPEAs reported in recent years. It can be seen that most of the MPEAs with heterostructured layers from LC and LSR exhibit much lower wear rates and smaller friction coefficients. While the wear resistance of MPEA components by SLM is rarely reported, it also deserves to be well studied.

Table 1. Comparison of the wear rates of some typical MPEAs at room temperature

Alloy	Wear conditions	Wear rate/(10^{-5} $mm^3 \cdot N^{-1} \cdot m^{-1}$)	CoF	Ref.
Homogenous CoCrFeMnNi	Ball-on-disc, Si_3N_4, 6 N, 0.1 m/s, 10 min	8	0.65	[137]
Homogenous CoCrFeMnNi	Pin-on-disc, Al_2O_3, 15 N, 0.1 m/s, 1,000 m	27.5	0.61	[138]
Homogenous MoNbTaVW	Pin-on-disc, Al_2O_3, 5 N, 0.1 m/s, 2,000 m	83	~ 0.5	[139]
Homogenous TiZrHfNb	Ball-on-disc, Si_3N_4 5 N, 0.035 m/s, 0.35 m/s, 60 min	17-22	0.42-0.62	[140]
Homogenous TiZrHfTaNb	Ball-on-disc, Si_3N_4 5 N, 0.035 m/s, 0.35 m/s, 60 min	5-25	0.46-0.65	[140]
Homogenous TiZrHfTaNb	Ball-on-disc, Si_3N_4 16 N, 24 N, 32 N 0.001 m/s, 25 min	3.41, 3.64, 3.83	0.29-0.30	[93]
Homogenous FeCoCrNi	Pin-on-disc, Al_2O_3, 2,000 g, 0.28 m/s, 60 min	16.83	0.41	[92]
LSR-TiZrHfTaNb	Ball-on-disc, Si_3N_4 16 N, 24 N, 32 N 0.001 m/s, 25 min	0.221, 0.238, 0.294	0.32-0.34	[93]
LSR-$AlCoCrFeNi_{2.1}$	Pin-on-disc, Al_2O_3, 4.9 N, 0.28 m/s, 504 m	~ 6	0.37	[100]
LSR-$FeCrCoNiTiAl_{0.6}$	Ball-on-disc, Al_2O_3, 5 N, 382 rpm/min, 83 min	1.375	0.14	[141]
LSR-$Al_2CoCrFeNiSi$	Ball-on-disc, Si_3N_4, 2 N, 120 mm/min, 30 min	0.032	0.24	[142]
LC-W/FeCoCrNi	Pin-on-disc, Al_2O_3, 2,000 g, 0.28 m/s, 60 min	12.47	0.37	[92]
LC-CoCrFeNiMn	Ball-on-disc, Si_3N_4, 5 N, 40 m/min, 30 min	0.107	0.22	[143]
LC-$CoCrFeNi_2V_{0.5}Ti_{0.75}$	Ball-on-disc, Si_3N_4, 15 N, 67 mm/s, 15 min	4.426	N/A	[144]
LC-NiCoCrMnFe	Ball-on-disc, Si_3N_4, 2 N, 2 Hz, 120 min	0.948	0.85	[145]
LC-FeCoCrNi-WC	Ball-on-disc, SiC, 50 N, 9 m/min, N/A	0.7	0.29	[146]
LC-AlCoCrFeNiTi	Ball-on-disc, Si_3N_4, 200 g, 500 r/min, 30 min	0.0013	N/A	[82]
LC-$AlCoCrFeNiTi_{0.8}$	Ball-on-disc, Si_3N_4, 5 N, 600 r/min, 30 min	0.136	0.64	[147]
LC-FeCrNiMnAl	Ball-on-disc, Si_3N_4, 35 N, 1 Hz, 30 min	0.007	0.46	[148]

SUMMARY AND PROSPECTS

In summary, heterostructured materials represent a significant advancement in materials science, offering unparalleled mechanical and functional properties through the strategic arrangement of different phases and structures. This review has highlighted several innovative techniques, including LST and LAM, which enable precise control over material microstructures. These technologies are particularly effective in creating specialized heterogeneous structures in MPEAs that can largely improve mechanical properties, such as gradient structures, dual-phase or multi-phase structures, core-shell structures, skeleton architectures, lamellar structures, nano precipitates, and hierarchical heterogeneous structures.

The tailored microstructures formed through these methods demonstrate remarkable improvements in properties such as strength-ductility synergy, fatigue resistance, and wear resistance. The ability to engineer materials at the micro- and nanoscale opens new avenues for developing high-performance MPEAs that are specifically tailored for a variety of applications. Despite these advancements, several challenges remain in achieving optimal and desired results for specific application scenarios and complicated serving environments.

(1) *Quality control.* Despite advancements in laser technology, ensuring product quality remains a challenge. Key issues include establishing optimal parameters to prevent defects such as porosity and cracks. Residual stress and anisotropy are still serious problems during the processing of MPEAs fabricated by laser-based techniques. While massive combinations involving laser power and scanning speed have been studied, a deeper understanding of interplays between processing parameters and feeding materials is in

prospect. Precise monitoring during manufacturing is crucial, as factors such as powder evaporation can adversely affect the final product. Consequently, post-processing techniques, such as heat treatment, are often essential to improve the sample quality and enhance material properties. Additionally, some innovative methods such as slurry-based laser powder bed fusion (s-LPBF)[149] and liquid-induced healing (LIH)[150] show promise in improving powder utilization and repairing micro-cracks, respectively, thus making it possible to further enhance the performance of MPEA in AM.

(2) *Advancing heterostructures.* Laser-prepared heterostructures offer unique opportunities but also face specific challenges. Traditional metal systems often achieve desired microstructures through processes such as hot extrusion, rolling, or forging. Some of the unique heterostructures are still difficult to replicate by laser-based techniques, including three-level heterogeneous grain structure fabricated by hot forging and cold rolling[151], as well as the heterogeneous lamella structure produced by asymmetric rolling[23]. Similarly, without the same force intervention in the preparation process as some traditional powder metallurgy methods, such as hot isostatic pressing or hot press sintering, the laser-based techniques still make it hard to prepare some bonding tightly bimodal composite materials with special components. Noticeably, the inherent properties of MPEAs present exciting possibilities, particularly with concepts such as chemical short-range order (CSRO)[152]. CSRO enhances mechanical properties and influences deformation mechanisms, and its understanding can lead to improved material performance[153]. More efforts are expected to focus on expanding the ability of laser-based techniques to create more unrealized heterostructures, thus optimizing the design or combinations of abundant heterostructures and exploring their potential applications.

(3) *Computational predictions.* The unique heterostructures achieved in the laser-fabricated MPEAs result from the complex thermal history during laser processing, featured by rapid cooling rates, high solidification speeds, and large temperature gradients[154], which is a complicated problem of multi-field coupling involving mechanical, thermal, and chemical fields. Besides, addressing application-level challenges is crucial for the successful deployment of laser-prepared heterostructured materials. Variability in service conditions necessitates the design of heterogeneous structures that ensure performance compatibility. The mechanistic understanding deepened by multi-phase field simulation, finite element analysis, and molecular dynamics should be paid more attention[155-158]; there remains a relative gap in research specifically addressing the unique challenges of laser-fabricated MPEA heterostructures. Advances in computational modeling and *in situ* characterization will play a vital role in tackling these issues. Effective models are necessary to be established with a successful arrangement of huge parameters involved in this complex physics-chemical problem, for better predicting both the evolution of each field during fabricating processes, and microstructures formed inside the components. Towards the specific application scenarios and constraints, optimized design of heterostructured metals is expected to be successfully obtained by time-saving and efficient simulation models and advanced machine learning technology.

As laser technology evolves, collaboration among materials scientists, engineers, and industry professionals will be essential for translating these innovations into practical applications, paving the way for next-generation high-performance structural metallic materials.

DECLARATIONS

Authors' contributions

Made the literature review and drafted the original version: Huang, J.; Hou, X.
Revised the manuscript: Yang, W.; Gao, Z.; Yang, X. S.

Conceived and supervised the project: Yang, X. S.

Availability of data and materials
Not applicable.

Financial support and sponsorship
This work was supported by the grants from the Research Grants Council of the Hong Kong Special Administrative Region, China (Nos. PolyU15210123 and PolyU15201424), PolyU grant (No. 1-CD4K), Guangdong Basic and Applied Basic Research Foundation (Nos. 2022A1515011322 and 2024A1515010781), and Fundamental Research Program of Shenzhen Science and Technology Innovation Commission (No. JCYJ20210324131405015). X Hou received a fellowship award from the Research Grants Council of the Hong Kong Special Administrative Region, China (Project No. PolyU PDFS2223-5S08). Z Gao and W Yang were supported by grants from the Research Committee of PolyU under student account codes RHVR and RK3J, respectively.

Conflicts of interest
Yang, X. S. is an Editorial Board Member of the journal *Microstructures* but was not involved in any steps of editorial processing, notably including reviewer selection, manuscript handling or decision-making, while the other authors have declared that they have no conflicts of interest.

Ethical approval and consent to participate
Not applicable.

Consent for publication
Not applicable.

REFERENCES
1. Ma, Y.; Yang, M.; Yuan, F.; Wu, X. A review on heterogeneous nanostructures: a strategy for superior mechanical properties in metals. *Metals* **2019**, *9*, 598. DOI
2. Yeh, J.; Chen, S.; Lin, S.; et al. Nanostructured high-entropy alloys with multiple principal elements: novel alloy design concepts and outcomes. *Adv. Eng. Mater.* **2004**, *6*, 299-303. DOI
3. Zhu, Y.; Wu, X. Heterostructured materials. *Prog. Mater. Sci.* **2023**, *131*, 101019. DOI
4. Cheng, Z.; Zhou, H.; Lu, Q.; Gao, H.; Lu, L. Extra strengthening and work hardening in gradient nanotwinned metals. *Science* **2018**, *362*, eaau1925. DOI PubMed
5. Pan, Q.; Zhang, L.; Feng, R.; et al. Gradient cell-structured high-entropy alloy with exceptional strength and ductility. *Science* **2021**, *374*, 984-9. DOI
6. Shang, Z.; Sun, T.; Ding, J.; et al. Gradient nanostructured steel with superior tensile plasticity. *Sci. Adv.* **2023**, *9*, eadd9780. DOI PubMed PMC
7. Zhang, Y.; He, C.; Yu, Q.; et al. Nacre-like surface nanolaminates enhance fatigue resistance of pure titanium. *Nat. Commun.* **2024**, *15*, 6917. DOI PubMed PMC
8. Bai, H.; Chen, Y.; Delattre, B.; Tomsia, A. P.; Ritchie, R. O. Bioinspired large-scale aligned porous materials assembled with dual temperature gradients. *Sci. Adv.* **2015**, *1*, e1500849. DOI PubMed PMC
9. Han, T.; Hou, C.; Zhao, Z.; et al. Simultaneous enhancement of strength and conductivity via self-assembled lamellar architecture. *Nat. Commun.* **2024**, *15*, 1863. DOI PubMed PMC
10. Wang, H.; Chen, D.; An, X.; et al. Deformation-induced crystalline-to-amorphous phase transformation in a CrMnFeCoNi high-entropy alloy. *Sci. Adv.* **2021**, *7*, eabe3105. DOI PubMed PMC
11. Gu, L.; Zhao, Y.; Li, Y.; et al. Ultrastrong and ductile medium-entropy alloys via hierarchical ordering. *Sci. Adv.* **2024**, *10*, eadn7553. DOI PubMed PMC
12. Duan, F.; Li, Q.; Jiang, Z.; et al. An order-disorder core-shell strategy for enhanced work-hardening capability and ductility in

nanostructured alloys. *Nat. Commun.* **2024**, *15*, 6832. DOI PubMed PMC

13. Ameyama, K.; Cazes, F.; Couque, H.; et al. Harmonic structure, a promising microstructure design. *Mater. Res. Lett.* **2022**, *10*, 440-71. DOI
14. Yang, W.; Luo, Z. P.; Bao, W. K.; Xie, H.; You, Z. S.; Jin, H. J. Light, strong, and stable nanoporous aluminum with native oxide shell. *Sci. Adv.* **2021**, *7*, eabb9471. DOI PubMed PMC
15. Vajpai, S. K.; Ota, M.; Zhang, Z.; Ameyama, K. Three-dimensionally gradient harmonic structure design: an integrated approach for high performance structural materials. *Mater. Res. Lett.* **2016**, *4*, 191-7. DOI
16. Fang, T. H.; Li, W. L.; Tao, N. R.; Lu, K. Revealing extraordinary intrinsic tensile plasticity in gradient nano-grained copper. *Science* **2011**, *331*, 1587-90. DOI PubMed
17. Ritchie, R. O. The conflicts between strength and toughness. *Nat. Mater.* **2011**, *10*, 817-22. DOI PubMed
18. Espinosa, H. D.; Rim, J. E.; Barthelat, F.; Buehler, M. J. Merger of structure and material in nacre and bone - perspectives on de novo biomimetic materials. *Prog. Mater. Sci.* **2009**, *54*, 1059-100. DOI
19. Zhao, F.; Sun, M.; Li, X.; Guo, F.; Li, M. The manufacturing technology of iron swords from the capital of the Han Empire in China. *SN. Appl. Sci.* **2020**, *2*, 3312. DOI
20. Yin, Z.; Yang, X.; Ma, X.; et al. Strength and ductility of gradient structured copper obtained by surface mechanical attrition treatment. *Mater. Des.* **2016**, *105*, 89-95. DOI
21. Gopalan, H.; Chokshi, A. H. The mechanical behavior of nacre across length scales. *J. Mech. Behav. Biomed. Mater.* **2018**, *78*, 96-107. DOI
22. Li, J.; Ma, X.; Lu, K.; Wang, Y.; Zhu, Y. Unusual deformation mechanisms evoked by hetero-zone interaction in a heterostructured FCC high-entropy alloy. *Acta. Mater.* **2025**, *282*, 120516. DOI
23. Wu, X.; Yang, M.; Yuan, F.; et al. Heterogeneous lamella structure unites ultrafine-grain strength with coarse-grain ductility. *Proc. Natl. Acad. Sci. USA.* **2015**, *112*, 14501-5. DOI PubMed PMC
24. Wu, X.; Zhu, Y. Gradient and lamellar heterostructures for superior mechanical properties. *MRS. Bull.* **2021**, *46*, 244-9. DOI
25. Zhu, Y. Introduction to heterostructured materials: a fast emerging field. *Metall. Mater. Trans. A.* **2021**, *52*, 4715-26. DOI
26. Zhu, Y.; Wu, X. Perspective on hetero-deformation induced (HDI) hardening and back stress. *Mater. Res. Lett.* **2019**, *7*, 393-8. DOI
27. Zhu, Y. T.; Liao, X. Nanostructured metals: retaining ductility. *Nat. Mater.* **2004**, *3*, 351-2. DOI PubMed
28. Zhu, Y.; Zhou, S.; Xiong, Z.; Liang, Y.; Xue, Y.; Wang, L. Enabling stronger eutectic high-entropy alloys with larger ductility by 3D printed directional lamellae. *Addit. Manuf.* **2021**, *39*, 101901. DOI
29. Liu, C.; Liu, Y.; Wang, Q.; et al. Nano-dual-phase metallic glass film enhances strength and ductility of a gradient nanograined magnesium alloy. *Adv. Sci.* **2020**, *7*, 2001480. DOI PubMed PMC
30. Zhu, W.; Gao, X.; Yao, Y.; et al. Nanostructured high entropy alloys as structural and functional materials. *ACS. Nano.* **2024**, *18*, 12672-706. DOI
31. Ma, Q. X.; Yang, H. J.; Wang, Z.; Shi, X. H.; Liaw, P. K.; Qiao, J. W. High strength and ductility in partially recrystallized $Fe_{40}Mn_{20}Cr_{20}Ni_{20}$ high-entropy alloys at cryogenic temperature. *Microstructures* **2022**, *2*, 2022015. DOI
32. Xiao, B.; Liu, S.; Zhang, J.; et al. Environmental embrittlement behavior of high-entropy alloys. *Microstructures* **2023**, *3*, 2023006. DOI
33. Xu, N.; Huang, Y.; Cao, Y.; Li, S.; Wang; Yd Novel casting CoCrNiAl eutectic high entropy alloys with high strength and good ductility. *Microstructures* **2023**, *3*, 2023015. DOI
34. Ying, H.; Yang, X.; He, H.; et al. Formation of strong and ductile FeNiCoCrB network-structured high-entropy alloys by fluxing. *Microstructures* **2023**, *3*, 2023018. DOI
35. Ren, J.; Zhang, Y.; Zhao, D.; et al. Strong yet ductile nanolamellar high-entropy alloys by additive manufacturing. *Nature* **2022**, *608*, 62-8. DOI
36. Cao, B.; Zhao, W.; Jing, L.; et al. Heterostructure high-entropy alloys with exceptional thermal stability and resistance towards intermediate temperature embrittlement. *J. Mater. Sci. Technol.* **2024**, *188*, 228-33. DOI
37. Zhu, Y.; Ameyama, K.; Anderson, P. M.; et al. Heterostructured materials: superior properties from hetero-zone interaction. *Mater. Res. Lett.* **2021**, *9*, 1-31. DOI
38. Ye, Y.; Wang, Q.; Lu, J.; Liu, C.; Yang, Y. High-entropy alloy: challenges and prospects. *Mater. Today.* **2016**, *19*, 349-62. DOI
39. Wang, Q.; Yang, Y.; Jiang, H.; Liu, C. T.; Ruan, H. H.; Lu, J. Superior tensile ductility in bulk metallic glass with gradient amorphous structure. *Sci. Rep.* **2014**, *4*, 4757. DOI PubMed PMC
40. Liu, Z.; Guo, S.; Liu, X.; et al. Micromechanical characterization of casting-induced inhomogeneity in an $Al_{0.8}$CoCrCuFeNi high-entropy alloy. *Scr. Mater.* **2011**, *64*, 868-71. DOI
41. Sarakinos, K.; Alami, J.; Konstantinidis, S. High power pulsed magnetron sputtering: a review on scientific and engineering state of the art. *Surf. Coat. Technol.* **2010**, *204*, 1661-84. DOI
42. Ma, Y.; Li, L.; Qian, J.; et al. Materials and structure engineering by magnetron sputtering for advanced lithium batteries. *Energy. Storage. Mater.* **2021**, *39*, 203-24. DOI
43. Liang, J.; Liu, Q.; Li, T.; et al. Magnetron sputtering enabled sustainable synthesis of nanomaterials for energy electrocatalysis. *Green. Chem.* **2021**, *23*, 2834-67. DOI
44. Costa, J. M.; Almeida, N. A. F. Ultrasound-assisted electrodeposition and synthesis of alloys and composite materials: a review. *Ultrason. Sonochem.* **2020**, *68*, 105193. DOI PubMed

45. Kale, M. B.; Borse, R. A.; Gomaa, A. M. A.; Wang, Y. Electrocatalysts by electrodeposition: recent advances, synthesis methods, and applications in energy conversion. *Adv. Funct. Mater.* **2021**, *31*, 2101313. DOI
46. Shi, Y.; Lee, C.; Tan, X.; et al. Atomic-level metal electrodeposition: synthetic strategies, applications, and catalytic mechanism in electrochemical energy conversion. *Small. Struct.* **2022**, *3*, 2100185. DOI
47. Lu, Y.; Dong, Y.; Guo, S.; et al. A promising new class of high-temperature alloys: eutectic high-entropy alloys. *Sci. Rep.* **2014**, *4*, 6200. DOI PubMed PMC
48. Shi, P.; Li, R.; Li, Y.; et al. Hierarchical crack buffering triples ductility in eutectic herringbone high-entropy alloys. *Science* **2021**, *373*, 912-8. DOI
49. Zheng, S.; Beyerlein, I. J.; Carpenter, J. S.; et al. High-strength and thermally stable bulk nanolayered composites due to twin-induced interfaces. *Nat. Commun.* **2013**, *4*, 1696. DOI
50. Majumdar J, Manna I. Laser material processing. *Int. Mater. Rev.* **2011**, *56*, 341-88. DOI
51. Lee, H.; Lim, C. H. J.; Low, M. J.; Tham, N.; Murukeshan, V. M.; Kim, Y. Lasers in additive manufacturing: a review. *Int. J. Precis. Eng. Manuf. Green. Technol.* **2017**, *4*, 307-22. DOI
52. Brighenti, R.; Cosma, M. P.; Marsavina, L.; Spagnoli, A.; Terzano, M. Laser-based additively manufactured polymers: a review on processes and mechanical models. *J. Mater. Sci.* **2021**, *56*, 961-98. DOI
53. Zhang, J.; Song, B.; Wei, Q.; Bourell, D.; Shi, Y. A review of selective laser melting of aluminum alloys: processing, microstructure, property and developing trends. *J. Mater. Sci. Technol.* **2019**, *35*, 270-84. DOI
54. Liu, H.; Lin, W.; Hong, M. Hybrid laser precision engineering of transparent hard materials: challenges, solutions and applications. *Light. Sci. Appl.* **2021**, *10*, 162. DOI PubMed PMC
55. Gu, D.; Shi, X.; Poprawe, R.; Bourell, D. L.; Setchi, R.; Zhu, J. Material-structure-performance integrated laser-metal additive manufacturing. *Science* **2021**, *372*, eabg1487. DOI PubMed
56. Jia, X.; Chen, Y.; Liu, L.; Wang, C.; Duan, J. Combined pulse laser: reliable tool for high-quality, high-efficiency material processing. *Opt. Laser. Technol.* **2022**, *153*, 108209. DOI
57. Ji, W.; Zhou, R.; Viveganantha, P.; See, W. M.; Gao, H.; Zhou, K. Recent progress in gradient-structured metals and alloys. *Prog. Mater. Sci.* **2023**, *140*, 101194. DOI
58. Yang, T.; Jia, Z.; Chen, H.; et al. Mechanical design of the highly porous cuttlebone: a bioceramic hard buoyancy tank for cuttlefish. *Proc. Natl. Acad. Sci. USA.* **2020**, *117*, 23450-9. DOI PubMed PMC
59. Huang, W.; Lin, X. Laser additive manufacturing of high-performance metal components. *Sci. Sin. Inf.* **2015**, *45*, 1111-26. DOI
60. Harish, V.; Ansari, M. M.; Tewari, D.; et al. Nanoparticle and nanostructure synthesis and controlled growth methods. *Nanomaterials* **2022**, *12*, 3226. DOI PubMed PMC
61. Zhu, K.; Vassel, A.; Brisset, F.; Lu, K.; Lu, J. Nanostructure formation mechanism of α-titanium using SMAT. *Acta. Mater.* **2004**, *52*, 4101-10. DOI
62. Zuo, J.; Lin, X. High-power laser systems. *Laser. Photonics. Rev.* **2022**, *16*, 2100741. DOI
63. Quazi, M. M.; Fazal, M. A.; Haseeb, A. S. M. A.; Yusof, F.; Masjuki, H. H.; Arslan, A. Laser-based surface modifications of aluminum and its alloys. *Crit. Rev. Solid. State. Mater. Sci.* **2016**, *41*, 106-31. DOI
64. Vorobyev, A. Y.; Guo, C. Direct femtosecond laser surface nano/microstructuring and its applications. *Laser. Photonics. Rev.* **2013**, *7*, 385-407. DOI
65. Zhang, Z.; Lin, P.; Zhou, H.; Ren, L. Microstructure, hardness, and thermal fatigue behavior of H21 steel processed by laser surface remelting. *Appl. Surf. Sci.* **2013**, *276*, 62-7. DOI
66. Wang, Z.; Lin, X.; Cao, Y.; Huang, W. Microstructure evolution in laser surface remelting of Ni-33wt.%Sn alloy. *J. Alloys. Compd.* **2013**, *577*, 309-14. DOI
67. Siddiqui, A. A.; Dubey, A. K. Recent trends in laser cladding and surface alloying. *Opt. Laser. Technol.* **2021**, *134*, 106619. DOI
68. Arif, Z. U.; Khalid, M. Y.; ur, R. E.; Ullah, S.; Atif, M.; Tariq, A. A review on laser cladding of high-entropy alloys, their recent trends and potential applications. *J. Manuf. Process.* **2021**, *68*, 225-73. DOI
69. Braisted, W. Finite element simulation of laser shock peening. *Int. J. Fatigue.* **1999**, *21*, 719-24. DOI
70. Liao, Y.; Suslov, S.; Ye, C.; Cheng, G. J. The mechanisms of thermal engineered laser shock peening for enhanced fatigue performance. *Acta. Mater.* **2012**, *60*, 4997-5009. DOI
71. Huang, D.; Dong, Y.; Chen, H.; Zhou, Y.; Zhang, M.; Yan, M. Effects of processing parameters on a β-solidifying TiAl alloy fabricated by laser-based additive manufacturing. *Microstructures* **2022**, *2*, 2022019. DOI
72. Dela Cruz, M. L.; Yakubov, V.; Li, X.; Ferry, M.; Zhang, M.; Yan, M. Microstructure evolution in laser powder bed fusion-built Fe-Mn-Si shape memory alloy. *Microstructures* **2023**, *3*, 2023012. DOI
73. Liu, Z.; Tan, Z.; Zhou, Z.; et al. Hot isostatic pressing induced precipitation strengthening at room and high temperature of Ni-Fe-Cr-Al-V high-entropy alloy manufactured by laser powder bed fusion. *Microstructures* **2024**, *4*, 2024024. DOI
74. Sefene, E. M. State-of-the-art of selective laser melting process: a comprehensive review. *J. Manu. Syst.* **2022**, *63*, 250-74. DOI
75. Yadroitsev, I.; Gusarov, A.; Yadroitsava, I.; Smurov, I. Single track formation in selective laser melting of metal powders. *J. Manuf. Process.* **2010**, *210*, 1624-31. DOI
76. Zhu, C.; Liu, T.; Qian, F.; et al. 3D printed functional nanomaterials for electrochemical energy storage. *Nano. Today.* **2017**, *15*, 107-20. DOI
77. Halani, P. R.; Kaya, I.; Shin, Y. C.; Karaca, H. E. Phase transformation characteristics and mechanical characterization of nitinol

synthesized by laser direct deposition. *Mater. Sci. Eng. A.* **2013**, *559*, 836-43. DOI

78. Eisenbarth, D.; Borges, E. P. M.; Wirth, F.; Wegener, K. Spatial powder flow measurement and efficiency prediction for laser direct metal deposition. *Surf. Coat. Technol.* **2019**, *362*, 397-408. DOI
79. Wilson, J. M.; Piya, C.; Shin, Y. C.; Zhao, F.; Ramani, K. Remanufacturing of turbine blades by laser direct deposition with its energy and environmental impact analysis. *J. Clean. Prod.* **2014**, *80*, 170-8. DOI
80. Bailey, N. S.; Katinas, C.; Shin, Y. C. Laser direct deposition of AISI H13 tool steel powder with numerical modeling of solid phase transformation, hardness, and residual stresses. *J. Mater. Process. Technol.* **2017**, *247*, 223-33. DOI
81. Zhang, Z.; Ma, Y.; Yang, M.; et al. Improving ductility by coherent nanoprecipitates in medium entropy alloy. *Int. J. Plasticity.* **2024**, *172*, 103821. DOI
82. Liu, H.; Liu, J.; Chen, P.; Yang, H. Microstructure and high temperature wear behaviour of in-situ TiC reinforced AlCoCrFeNi-based high-entropy alloy composite coatings fabricated by laser cladding. *Opt. Laser. Technol.* **2019**, *118*, 140-50. DOI
83. Thevamaran, R.; Lawal, O.; Yazdi, S.; Jeon, S. J.; Lee, J. H.; Thomas, E. L. Dynamic creation and evolution of gradient nanostructure in single-crystal metallic microcubes. *Science* **2016**, *354*, 312-6. DOI PubMed
84. Lou, L.; Li, Y.; Li, X.; et al. Directional magnetization reversal enables ultrahigh energy density in gradient nanostructures. *Adv. Mater.* **2021**, *33*, e2102800. DOI
85. Gou, S.; Li, S.; Hu, H.; et al. Surface hardening of CrCoFeNi high-entropy alloys via Al laser alloying. *Mater. Res. Lett.* **2021**, *9*, 437-44. DOI
86. Fu, W.; Huang, Y.; Sun, J.; Ngan, A. H. Strengthening $CrFeCoNiMn_{0.75}Cu_{0.25}$ high entropy alloy via laser shock peening. *Int. J. Plasticity.* **2022**, *154*, 103296. DOI
87. Yuan, S.; Gao, Z.; Fu, H.; Cheung, C. F.; Yang, X. Superior corrosion-resistant nanostructured hypoeutectic CrCoNi-based medium-entropy alloy processed by laser surface remelting. *J. Alloys. Compd.* **2023**, *967*, 171802. DOI
88. Zhang, B.; Chen, J.; Wang, P.; Sun, B.; Cao, Y. Enhanced strength-ductility of CoCrFeMnNi high-entropy alloy with inverse gradient-grained structure prepared by laser surface heat-treatment technique. *J. Mater. Sci. Technol.* **2022**, *111*, 111-9. DOI
89. Shen, J.; Choi, Y. T.; Yang, J.; et al. Fabrication of spatially-variable heterostructured CoCrFeMnNi high entropy alloy by laser processing. *Mater. Sci. Eng. A.* **2024**, *896*, 146272. DOI
90. Gu, G. H.; Kim, E. S.; Kwon, H.; et al. Fabrication of multi-gradient heterostructured CoCrFeMnNi high-entropy alloy using laser metal deposition. *Mater. Sci. Eng. A.* **2022**, *836*, 142718. DOI
91. Dobbelstein, H.; Gurevich, E. L.; George, E. P.; Ostendorf, A.; Laplanche, G. Laser metal deposition of compositionally graded TiZrNbTa refractory high-entropy alloys using elemental powder blends. *Addit. Manuf.* **2019**, *25*, 252-62. DOI
92. Guan, Y.; Chen, D.; Cui, X.; et al. A novel W/FeCoCrNi-based in-situ formed high-entropy alloy gradient coating with Laves-FCC dual-phase structure and synergistic friction behavior. *Tribol. Int.* **2024**, *192*, 109228. DOI
93. Luo, J.; Sun, W.; Duan, R.; et al. Laser surface treatment-introduced gradient nanostructured TiZrHfTaNb refractory high-entropy alloy with significantly enhanced wear resistance. *J. Mater. Sci. Technol.* **2022**, *110*, 43-56. DOI
94. Zhang, Q.; Chen, Z.; Dong, Y.; Li, C.; Wang, Y. High strength and ductility eutectic high entropy alloy with unique core-shell structure. *J. Alloys. Compd.* **2024**, *976*, 173141. DOI
95. Kumar, P.; Huang, S.; Cook, D. H.; et al. A strong fracture-resistant high-entropy alloy with nano-bridged honeycomb microstructure intrinsically toughened by 3D-printing. *Nat. Commun.* **2024**, *15*, 841. DOI PubMed PMC
96. Mu, Y.; He, L.; Deng, S.; et al. A high-entropy alloy with dislocation-precipitate skeleton for ultrastrength and ductility. *Acta. Mater.* **2022**, *232*, 117975. DOI
97. Huang, L.; Sun, Y.; Chen, N.; et al. Simultaneously enhanced strength-ductility of $AlCoCrFeNi_{2.1}$ eutectic high-entropy alloy via additive manufacturing. *Mater. Sci. Eng. A.* **2022**, *830*, 142327. DOI
98. Sun, Y.; Zhang, C.; Ning, Z.; Sun, J.; Ngan, A. H.; Huang, Y. Additively manufactured low-gradient interfacial heterostructured medium-entropy alloy multilayers with superior strength and ductility synergy. *Compos. Part. B. Eng.* **2024**, *280*, 111522. DOI
99. Mu, Y.; Sun, K.; Jia, Y.; et al. 3D-printed strong and ductile high-entropy alloys with orientation arranged nanostructure complex. *J. Alloys. Compd.* **2023**, *968*, 171824. DOI
100. Miao, J.; Yao, H.; Wang, J.; Lu, Y.; Wang, T.; Li, T. Surface modification for $AlCoCrFeNi_{2.1}$ eutectic high-entropy alloy via laser remelting technology and subsequent aging heat treatment. *J. Alloys. Compd.* **2022**, *894*, 162380. DOI
101. Luo, J.; Sun, W.; Liang, D.; et al. An ultra-strong and ductile crystalline-amorphous nanostructured surface layer on $TiZrHfTaNb_{0.2}$ high-entropy alloy by laser surface processing. *Mater. Des.* **2023**, *227*, 111710. DOI
102. Park, J. M.; Asghari-rad, P.; Zargaran, A.; et al. Nano-scale heterogeneity-driven metastability engineering in ferrous medium-entropy alloy induced by additive manufacturing. *Acta. Mater.* **2021**, *221*, 117426. DOI
103. Wu, Y.; Cai, Y.; Wang, T.; et al. A refractory $Hf_{25}Nb_{25}Ti_{25}Zr_{25}$ high-entropy alloy with excellent structural stability and tensile properties. *Mater. Lett.* **2014**, *130*, 277-80. DOI
104. He, J.; Liu, W.; Wang, H.; et al. Effects of Al addition on structural evolution and tensile properties of the FeCoNiCrMn high-entropy alloy system. *Acta. Mater.* **2014**, *62*, 105-13. DOI
105. Gludovatz, B.; Hohenwarter, A.; Catoor, D.; Chang, E. H.; George, E. P.; Ritchie, R. O. A fracture-resistant high-entropy alloy for cryogenic applications. *Science* **2014**, *345*, 1153-8. DOI PubMed
106. Lu, Y.; Wu, S.; Gan, Y.; et al. Investigation on the microstructure, mechanical property and corrosion behavior of the selective laser melted CoCrW alloy for dental application. *Mater. Sci. Eng. C. Mater. Biol. Appl.* **2015**, *49*, 517-25. DOI

107. Senkov, O.; Semiatin, S. Microstructure and properties of a refractory high-entropy alloy after cold working. *J. Alloys. Compd.* **2015**, *649*, 1110-23. DOI
108. Liu, W.; He, J.; Huang, H.; Wang, H.; Lu, Z.; Liu, C. Effects of Nb additions on the microstructure and mechanical property of CoCrFeNi high-entropy alloys. *Intermetallics* **2015**, *60*, 1-8. DOI
109. Brif, Y.; Thomas, M.; Todd, I. The use of high-entropy alloys in additive manufacturing. *Scr. Mater.* **2015**, *99*, 93-6. DOI
110. Niu, S.; Kou, H.; Guo, T.; Zhang, Y.; Wang, J.; Li, J. Strengthening of nanoprecipitations in an annealed $Al_{0.5}$CoCrFeNi high entropy alloy. *Mater. Sci. Eng. A.* **2016**, *671*, 82-6. DOI
111. Yoshida, S.; Bhattacharjee, T.; Bai, Y.; Tsuji, N. Friction stress and hall-petch relationship in CoCrNi equi-atomic medium entropy alloy processed by severe plastic deformation and subsequent annealing. *Sc. Mater.* **2017**, *134*, 33-6. DOI
112. Huang, H.; Wu, Y.; He, J.; et al. Phase-transformation ductilization of brittle high-entropy alloys via metastability engineering. *Adv. Mater.* **2017**, *29*, 1701678. DOI
113. Zhu, Z.; Nguyen, Q.; Ng, F.; et al. Hierarchical microstructure and strengthening mechanisms of a CoCrFeNiMn high entropy alloy additively manufactured by selective laser melting. *Scr. Mater.* **2018**, *154*, 20-4. DOI
114. Peyrouzet, F.; Hachet, D.; Soulas, R.; Navone, C.; Godet, S.; Gorsse, S. Selective laser melting of $Al_{0.3}$CoCrFeNi high-entropy alloy: printability, microstructure, and mechanical properties. *JOM.* **2019**, *71*, 3443-51. DOI
115. Zhu, Z. G.; An, X. H.; Lu, W. J.; et al. Selective laser melting enabling the hierarchically heterogeneous microstructure and excellent mechanical properties in an interstitial solute strengthened high entropy alloy. *Mater. Res. Lett.* **2019**, *7*, 453-9. DOI
116. Yao, H.; Tan, Z.; He, D.; et al. High strength and ductility AlCrFeNiV high entropy alloy with hierarchically heterogeneous microstructure prepared by selective laser melting. *J. Alloys. Compd.* **2020**, *813*, 152196. DOI
117. Kim, Y.; Baek, M.; Yang, S.; Lee, K. In-situ formed oxide enables extraordinary high-cycle fatigue resistance in additively manufactured CoCrFeMnNi high-entropy alloy. *Addit. Manuf.* **2021**, *38*, 101832. DOI
118. Yao, N.; Lu, T.; Feng, K.; et al. Ultrastrong and ductile additively manufactured precipitation-hardening medium-entropy alloy at ambient and cryogenic temperatures. *Acta. Mater.* **2022**, *236*, 118142. DOI
119. Wu, Y.; Zhao, X.; Chen, Q.; et al. Strengthening and fracture mechanisms of a precipitation hardening high-entropy alloy fabricated by selective laser melting. *Virtual. Phys. Prototyp.* **2022**, *17*, 451-67. DOI
120. Lu, Y.; Wu, X.; Fu, Z.; et al. Ductile and ultrahigh-strength eutectic high-entropy alloys by large-volume 3D printing. *J. Mater. Sci. Technol.* **2022**, *126*, 15-21. DOI
121. Liu, X.; Hu, R.; Lu, W.; et al. Temperature-dependent tensile deformation and plasticity loss mechanism of a novel Ni-Cr-W-based superalloy prepared by laser powder bed fusion. *Addit. Manuf.* **2023**, *78*, 103883. DOI
122. Fu, W.; Sun, Y.; Fan, G.; et al. Strain delocalization in a gradient-structured high entropy alloy under uniaxial tensile loading. *Int. J. Plasticity.* **2023**, *171*, 103808. DOI
123. Kim, R. E.; Gu, G. H.; Choi, Y. T.; Lee, J. A.; Kim, H. S. Superior tensile properties and formability synergy of high-entropy alloys through inverse-gradient structures via laser surface treatment. *Scr. Mater.* **2023**, *234*, 115587. DOI
124. Jiao, M.; Lei, Z.; Wu, Y.; et al. Manipulating the ordered oxygen complexes to achieve high strength and ductility in medium-entropy alloys. *Nat. Commun.* **2023**, *14*, 806. DOI PubMed PMC
125. Ren, J.; Wu, M.; Li, C.; et al. Deformation mechanisms in an additively manufactured dual-phase eutectic high-entropy alloy. *Acta. Mater.* **2023**, *257*, 119179. DOI
126. Zhang, W.; Chabok, A.; Wang, H.; et al. Ultra-strong and ductile precipitation-strengthened high entropy alloy with 0.5% Nb addition produced by laser additive manufacturing. *J. Mater. Sci. Technol.* **2024**, *187*, 195-211. DOI
127. Singh, P.; Johnson, D. D.; Tiarks, J.; et al. Theory-guided design of duplex-phase multi-principal-element alloys. *Acta. Mater.* **2024**, *272*, 119952. DOI
128. Li, X.; Lu, L.; Li, J.; Zhang, X.; Gao, H. Mechanical properties and deformation mechanisms of gradient nanostructured metals and alloys. *Nat. Rev. Mater.* **2020**, *5*, 706-23. DOI
129. Sathiyamoorthi, P.; Kim, H. S. High-entropy alloys with heterogeneous microstructure: processing and mechanical properties. *Prog. Mater. Sci.* **2022**, *123*, 100709. DOI
130. Ma, E.; Zhu, T. Towards strength-ductility synergy through the design of heterogeneous nanostructures in metals. *Mater. Today.* **2017**, *20*, 323-31. DOI
131. Hart, E. Theory of the tensile test. *Acta. Metall.* **1967**, *15*, 351-5. DOI
132. Hutchinson, J.; Neale, K. Influence of strain-rate sensitivity on necking under uniaxial tension. *Acta. Metall.* **1977**, *25*, 839-46. DOI
133. Peng, J.; Li, L.; Li, F.; et al. The predicted rate-dependent deformation behaviour and multistage strain hardening in a model heterostructured body-centered cubic high entropy alloy. *Int. J. Plasticity.* **2021**, *145*, 103073. DOI
134. Yang, L.; Lu, L. The influence of sample thickness on the tensile properties of pure Cu with different grain sizes. *Scr. Mater.* **2013**, *69*, 242-5. DOI
135. Jin, M.; Hosseini, E.; Holdsworth, S.; Pham, M. Thermally activated dependence of fatigue behaviour of CrMnFeCoNi high entropy alloy fabricated by laser powder-bed fusion. *Addit. Manuf.* **2022**, *51*, 102600. DOI
136. Chen, Y.; Li, B.; Chen, B.; Xuan, F. High-cycle fatigue induced twinning in CoCrFeNi high-entropy alloy processed by laser powder bed fusion additive manufacturing. *Addit. Manuf.* **2023**, *61*, 103319. DOI
137. Nagarjuna, C.; You, H.; Ahn, S.; et al. Worn surface and subsurface layer structure formation behavior on wear mechanism of CoCrFeMnNi high entropy alloy in different sliding conditions. *App. Surf. Sci.* **2021**, *549*, 149202. DOI

138. Joseph, J.; Haghdadi, N.; Shamlaye, K.; Hodgson, P.; Barnett, M.; Fabijanic, D. The sliding wear behaviour of CoCrFeMnNi and AlxCoCrFeNi high entropy alloys at elevated temperatures. *Wear* **2019**, *428-9*, 32-44. DOI
139. Poulia, A.; Georgatis, E.; Lekatou, A.; Karantzalis, A. Dry-sliding wear response of MoTaWNbV high entropy alloy. *Adv. Eng. Mater.* **2017**, *19*, 1600535. DOI
140. Sadeghilaridjani, M.; Pole, M.; Jha, S.; Muskeri, S.; Ghodki, N.; Mukherjee, S. Deformation and tribological behavior of ductile refractory high-entropy alloys. *Wear* **2021**, *478-9*, 203916. DOI
141. Chen, L.; He, D.; Han, B.; et al. Effect of laser remelting on wear behavior of HVOF-sprayed $FeCrCoNiTiAl_{0.6}$ high entropy alloy coating. *Appl. Sci.* **2020**, *10*, 7211. DOI
142. Jin, B.; Zhang, N.; Yu, H.; Hao, D.; Ma, Y. AlxCoCrFeNiSi high entropy alloy coatings with high microhardness and improved wear resistance. *Surf. Coat. Technol.* **2020**, *402*, 126328. DOI
143. Du, J.; Xu, X.; Zhang, H.; et al. Microstructure and wear resistance of CoCrFeNiMn coatings prepared by extreme-high-speed laser cladding. *Surf. Coat. Technol.* **2023**, *470*, 129821. DOI
144. Li, Y.; Liang, H.; Nie, Q.; et al. Microstructures and wear resistance of $CoCrFeNi_2V_{0.5}Ti_x$ high-entropy alloy coatings prepared by laser cladding. *Crystals* **2020**, *10*, 352. DOI
145. Shi, F.; Zhang, Q.; Xu, C.; et al. In-situ synthesis of NiCoCrMnFe high entropy alloy coating by laser cladding. *Opt. Laser. Technol.* **2022**, *151*, 108020. DOI
146. Peng, Y.; Zhang, W.; Li, T.; et al. Microstructures and mechanical properties of FeCoCrNi high entropy alloy/WC reinforcing particles composite coatings prepared by laser cladding and plasma cladding. *Int. J. Refract. Metals. Hard. Mater.* **2019**, *84*, 105044. DOI
147. Liu, H.; Liu, J.; Li, X.; Chen, P.; Yang, H.; Hao, J. Effect of heat treatment on phase stability and wear behavior of laser clad $AlCoCrFeNiTi_{0.8}$ high-entropy alloy coatings. *Surf. Coat. Technol.* **2020**, *392*, 125758. DOI
148. Rui, H.; Meiping, W.; Chen, C.; Dadong, J.; Yuling, G.; Xiaojin, M. Microstructure evolution, mechanical properties of FeCrNiMnAl high entropy alloy coatings fabricated by laser cladding. *Surf. Coat. Technol.* **2022**, *447*, 128851. DOI
149. Meyers, S.; Gurung, K.; Kinds, Y.; Hooreweder, B. V. On the use of slurry as an alternative to dry powder for laser powder bed fusion of 316L stainless steel. *Addit. Manuf. Lett.* **2024**, *11*, 100230. DOI
150. Hu, X.; Guo, C.; Huang, Y.; et al. Liquid-induced healing of cracks in nickel-based superalloy fabricated by laser powder bed fusion. *Acta. Mater.* **2024**, *267*, 119731. DOI
151. Yang, M.; Yan, D.; Yuan, F.; Jiang, P.; Ma, E.; Wu, X. Dynamically reinforced heterogeneous grain structure prolongs ductility in a medium-entropy alloy with gigapascal yield strength. *Proc. Natl. Acad. Sci. USA.* **2018**, *115*, 7224-9. DOI PubMed PMC
152. Chen, X.; Wang, Q.; Cheng, Z.; et al. Direct observation of chemical short-range order in a medium-entropy alloy. *Nature* **2021**, *592*, 712-6. DOI
153. Han, Y.; Chen, H.; Sun, Y.; et al. Ubiquitous short-range order in multi-principal element alloys. *Nat. Commun.* **2024**, *15*, 6486. DOI PubMed PMC
154. Karthik, G. M.; Kim, H. S. Heterogeneous aspects of additive manufactured metallic parts: a review. *Met. Mater. Int.* **2021**, *27*, 1-39. DOI
155. Yang, Y.; Ragnvaldsen, O.; Bai, Y.; Yi, M.; Xu, B. 3D non-isothermal phase-field simulation of microstructure evolution during selective laser sintering. *NPJ. Comput. Mater.* **2019**, *5*, 219. DOI
156. Qian, L.; Yang, W.; Luo, J.; Wang, Y.; Chan, K. C.; Yang, X. S. Amorphous thickness-dependent strengthening-softening transition in crystalline-amorphous nanocomposites. *Nano. Lett.* **2023**, *23*, 11288-96. DOI
157. Qian, L.; Wu, B.; Fu, H.; et al. Atomistic simulations of the enhanced creep resistance and underlying mechanisms of nanograined-nanotwinned copper. *Mater. Sci. Eng. A.* **2022**, *855*, 143912. DOI
158. Chen, X.; Liu, L.; Gao, R.; Lu, S.; Fu, T. Molecular dynamics simulation of the heterostructure of the CoCrFeMnNi high entropy alloy under an impact load. *Model. Simul. Mater. Sci. Eng.* **2023**, *31*, 085020. DOI